МІНІСТЕРСТВО ОСВІТИ І НАУКИ УКРАЇНИ

НАЦІОНАЛЬНИЙ АВІАЦІЙНИЙ УНІВЕРСИТЕТ

КАФЕДРА КОНСТРУКЦІЇ ЛІТАЛЬНИХ АПАРАТІВ

ДОПУСТИТИ ДО ЗАХИСТУ
Завідувач кафедри
д.т.н., професор
_____ Сергій ІГНАТОВИЧ
«___» _____ 2022 р.

КВАЛІФІКАЦІЙНА РОБОТА
ВИПУСКНИКА ОСВІТНЬОГО СТУПЕНЯ МАГІСТРА
ЗІ СПЕЦІАЛЬНОСТІ
«АВІАЦІЙНА ТА РАКЕТНО-КОСМІЧНА ТЕХНІКА»

Тема: «Перспективи використання лазерного селективного плавлення сплавів Al/Ti»

Виконавець: _____ **Яньфей ВАН**

Керівник: к.т.н., доцент _____ **Володимир КРАСНОПОЛЬСЬКИЙ**

Охорона праці: к.т.н., доцент _____ **Катерина КАЖАН**

Охорона навколишнього середовища:

к.т.н., професор _____ **Леся ПАВЛЮХ**

Нормоконтролер: к.т.н., доцент _____ **Володимир КРАСНОПОЛЬСЬКИЙ**

Київ 2022

MINISTRY OF EDUCATION AND SCIENCE OF UKRAINE

NATIONAL AVIATION UNIVERSITY

DEPARTMENT OF AIRCRAFT DESIGN

PERMISSION TO DEFEND
Head of the department,
Dr. of Sc., professor
_____ Sergiy IGNATOVYCH
"___" _____ 2022

MASTER DEGREE THESIS
ON SPECIALITY
"AVIATION AND ROCKET-SPACE TECHNOLOGIES"

Topic: "Perspectives of laser selective melting usage for Al/Ti alloys"

Fulfilled by:	**_____**	**Yanfei WANG**
Supervisor: **PhD, associate professor**	**_____**	**Volodymyr KRASNOPOLSKYI**
Labor protection advisor: **PhD, associate professor**	**_____**	**Katerina KAZHAN**
Environmental protection adviser: **PhD, professor**	**_____**	**Lesya PAVLYUKH**
Standards inspector: **PhD, associate professor**	**_____**	**Volodymyr KRASNOPOLSKYI**

Kyiv 2022

НАЦІОНАЛЬНИЙ АВІАЦІЙНИЙ УНІВЕРСИТЕТ

Факультет аерокосмічний
Кафедра конструкції літальних апаратів
Освітній ступінь «Магістр»
Спеціальність 134 «Авіаційна та ракетно-космічна техніка»
Освітньо-професійна програма «Обладнання повітряних суден»

ЗАТВЕРДЖУЮ
Завідувач кафедри д.т.н., проф.

_____ Сергій ІГНАТОВИЧ
«___»_____2022 р.

ЗАВДАННЯ

на виконання кваліфікаційної роботи пошукача

Яньфей ВАН

1. Тема роботи **«**Перспективи використання лазерного селективного плавлення сплавів Al/Ti**»**, затверджена наказом ректора від 05 жовтня 2022 року №1861/ст.

2. Термін виконання роботи: з 06 жовтня 2022 р. по 30 листопада 2022 р.

3. Вихідні дані до роботи: Встановіть потужність лазера на 230 Вт, 290 Вт, 350 Вт, швидкість сканування суцільної поверхні на 1100 мм/с, 1300 мм/с, 1500 мм/с, швидкість сканування контуру на 700, 900, 1100 мм/с і інтервал сканування на 0,15 мм, 0,17 мм, 0,19 мм.

4. Зміст пояснювальної записки: основна частина: Аналіз поточного стану СЛМ, Експериментальні матеріали, обладнання та методи випробувань; Вплив параметрів процесу та положення формування на точність розмірів та шорсткість поверхні сплаву $AlSi_{10}Mg/TiB_2$ для формування SLM. особлива частина: Охорона праці, Охорона навколишнього середовища.

5. Перелік обов’язкового графічного (ілюстративного) матеріалу: презентація Power Point, малюнки та схеми.

6. Календарний план-графік:

№	Завдання	Термін виконання	Відмітка про виконання
1	Отримання завдання, обробка статистичних даних.	06.10.2022 – 20.10.2022	
2	Проведіть відповідні експерименти. Ефективність досліджуваного зразка.	21.10.2022 – 29.10.2022	
3	Дизайн оптимізації експерименту. Експериментальний аналіз і теоретична верифікаці.	30.10.2022 – 01.11.2022	
4	Охорона праці.	01.10.2022 – 03.10.2022	
5	Охорона навколишнього середовища.	04.11.2022 – 06.11.2022	
6	Оформлення кваліфікаційної роботи.	06.11.2022 – 10.11.2022	

7. Консультанти з окремих розділів:

Розділ	Консультанти	Дата, підпис	
		Завдання видав	Завдання прийняв
Охорона праці	к.т.н., доцент Катерина КАЖАН		
Охорона навколишнього середовища	к.т.н., професор Леся ПАВЛЮХ		

8. Дата видачі завдання: 5 жовтня 2022 р.

Керівник кваліфікаційної роботи: _____ Володимир КРАСНОПОЛЬСЬКИЙ

Завдання прийняв до виконання: _____ Яньфей ВАН

NATIONAL AVIATION UNIVERSITY

Aerospace Faculty
Department of Aircraft Design
Educational Degree "Master"
Specialty 134 "Aviation and Rocket-Space Technologies"
Educational Professional Program "Aircraft Equipment"

APPROVED BY
Head of Department, Dr. of Sc., prof.
_____Sergiy IGNATOVYCH
"___"_____2022

TASK
for the master degree thesis
Yanfei WANG

1. Topic: "Perspectives of laser selective melting usage for Al/Ti alloys", approved by the Rector's order № 1861/ст from 05 October 2022 year.

2. Period of work execution: from 05 October 2022 year to 30 November 2022 year.

3. Initial data: Set the laser power to 230 W, 290 W, 350 W, the solid scan speed to 1100 mm/s, 1300 mm/s, 1500 mm/s, the contour scan speed to 700, 900, 1100 mm/s, and the scan spacing to 0.15 mm, 0.17 mm, 0.19 mm.

4. Content: Introduction; main part: Analysis of SLM present situation, Experimental materials, equipment and test methods; Influence of process parameters and forming position on the dimensional accuracy and surface roughness of SLM forming $AlSi_{10}Mg/TiB_2$ alloy. special part: Labor protection, Environmental protection.

5. Required material: Power Point Presentation, drawings and diagrams.

6.Thesis schedule:

№	Task	Time limits	Done
1	Task receiving, processing of statistical data.	06.10.2022 – 20.10.2022	
2	Carry out related experiments. Test specimen performance.	21.10.2022 – 29.10.2022	
3	Experiment optimization design. Experimental analysis and theoretical verification.	30.10.2022 – 01.11.2022	
4	Labor protection .	01.11.2022 – 03.11.2022	
5	Environmental protection.	04.11.2022 – 06.11.2022	
6	Edit and correct the draft, modify the format	06.11.2022 – 10.11.2022	

7. Special chapter advisers:

Chapter	Adviser	Date, signature	
		Task issued	Task received
Labor protection	PhD, associate professor Katerina KAZHAN		
Environmental protection	PhD, professor Lesya PAVLYUKH		

8. Date of issue of the task: 8 September 2022 year.

Supervisor: _____ Volodymyr KRASNOPOLSKII

Student: _____ Yanfei WANG

РЕФЕРАТ

Магістерська робота «Перспективи використання лазерного селективного плавлення сплавів Al/Ti»

74 с., 40 рис., 7табл., 37 джерел

Основний зміст дослідження цієї роботи полягає в оптимізації параметрів процесу лазерного селективного формування плавленням порошку алюмінієвого сплаву $AlSi_{10}Mg/TiB_2$ та дослідженні впливу напрямку друку фасонних деталей на точність розмірів і шорсткість поверхні. В роботі досліджувалися точність розмірів і шорсткість поверхні сформованих деталей, оптимальні параметри процесу селективного лазерного формування плавленням, вплив параметрів процесу лазерного селективного формування плавленням на формувальні деталі при різних напрямках друку та ефект TiB_2 наночастинок на точність розмірів і шорсткість поверхні формованих деталей.

З метою вивчення впливу різних параметрів процесу (потужності лазера, швидкості сканування, товщини порошку тощо) на точність розмірів і шорсткість поверхні формованих деталей шляхом лазерного селективного плавлення та формування, ортогональний експеримент спочатку використовувався для дослідження параметрів процесу, які мають найбільший вплив на шорсткість і точність розмірів. Знайдені найкращі параметри процесу для точності розмірів і шорсткості поверхні сформованих деталей.

Отримавши найкращі параметри процесу формування, досліджені різні напрямки друку сформованих деталей, які впливають на точність розмірів та шорсткість поверхні сформованих деталей і знайдений найкращий напрямок друку.

SLM, точність розмірів, шорсткість поверхні, щільність, наночастинки

ABSTRACT

Master thesis "Perspectives of laser selective melting usage for Al/Ti alloys"

74 pages, 40 figures, 7 tables, 37 references

The main research contents of this paper are optimization of process parameters for laser selective melting forming of $AlSi_{10}Mg/TiB_2$ aluminum alloy powder and the influence of the printing direction of the formed parts on the dimensional accuracy and surface roughness. In the work were explored the dimensional accuracy and surface roughness of the formed parts and the optimal process parameters of the selective laser melting forming, the influence of the laser selective melting forming process parameters on the forming parts under different printing directions, and the effect of TiB_2 nanoparticles on the dimensional accuracy and surface roughness of the formed parts.

Aiming at the influence of different process parameters (laser power, scanning speed, powder thickness, etc.) on the dimensional accuracy and surface roughness of the formed parts by laser selective melting and forming, the orthogonal experiment was firstly used to explore the process parameters that have the greatest influence on the roughness and dimensional accuracy. Found out the best process parameters for the dimensional accuracy and surface roughness of the formed parts.

After obtaining the best forming process parameters, explore the different printing directions of the formed parts, which affect the surface dimensional accuracy and surface roughness of the formed parts, and find the best printing direction of the formed parts.

SLM, dimensional accuracy, surface roughness, density, nanoparticles

CONTENT

INTRODUCTION

With the increasing pursuit of large-scale, lightweight, long-life and high reliability of aerospace structural parts, the demand for high-speed and lightweight modern transportation equipment and rails has vigorously promoted the research and development and application of aluminum alloys of different types, different performances and different industries. Among them, $AlSi_{10}Mg$ aluminum alloy is one of the most commonly used casting Al-Si alloys, its mechanical properties and melting and casting process are excellent, so it is in great demand in aviation, aerospace and transportation industries. Casting is the most commonly used process method for preparing $AlSi_{10}Mg$ aluminum alloy forming parts, the main problem in the current production is that there are more casting defects such as pores and shrinkage porosity, resulting in low mechanical properties, such as tensile strength of 300MPa, elongation of about 3%, and long production cycle, which is not conducive to product upgrading. Selective Laser Melting (SLM) technology can first generate a three-dimensional model of the part and use slicing software for auxiliary sectioning, and then directly clean form the metal powder to achieve high strength and high toughness of complex structural parts, compared with traditional processing, SLM technology has many unique advantages, studies have shown , SLM forming AlSi10Mg aluminum alloy specimen tensile strength up to 400 MPa, elongation up to 5.7%, The performance is significantly higher than the casting level. SLM technology mainly includes stainless steel powder, titanium alloy powder, aluminum alloy powder, superalloy powder and other forming materials. However, due to the characteristics of light weight, easy oxidation and high reflectivity of aluminum alloy, SLM formed aluminum alloy parts still have problems such as low dimensional accuracy and poor surface roughness compared with stainless steel powder, titanium alloy powder, superalloy and other forming materials.

PART 1. ANALYSIS OF SLM PRESENT SITUATION

1.1 Overview of selective laser melting technology

Selective Laser Melting (SLM) technology is a manufacturing technology developed on the basis of prototype manufacturing technology [1]. First, it is necessary to model and slice the parts in three dimensions through special software to form an ordered two-dimensional thin layer in a certain direction, and then use the powder laying system to spread powder layer by layer on the printing substrate, and then use a high-energy laser beam to scan the metal powder layer by layer according to the contour data, selectively melt and quickly solidify the metal powder, and finally realize the manufacture of three-dimensional solid in the way of layer by layer accumulation [2].

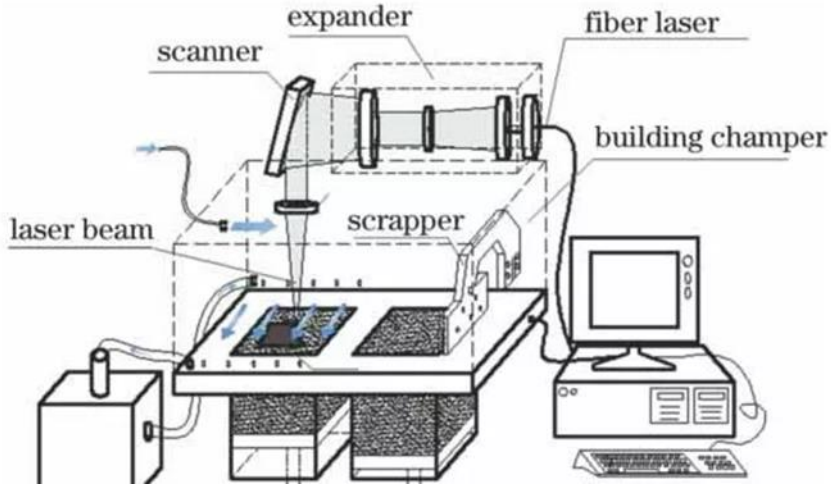

Fig. 1.1. Schematic diagram of SLM forming principle.

SLM forming technology has many advantages over traditional manufacturing processes, and its advanced nature is mainly reflected in the following aspects [3,4,5]:

1) Almost any shape of parts can be formed, the degree of freedom of part design is high, and it has great advantages in the forming of personalized customized parts;

2) Can be directly formed without the need for a mold, which can save time and cost;

3) Powder materials can be recycled and reused, which is a green manufacturing method.

The quality issues that SLM molded parts need to pay attention to include: porosity, cracks, warpage, dimensional accuracy, surface roughness and mechanical properties, etc., these quality problems are also affected by many factors, which can be mainly divided into two categories: powder properties and processing parameters. Each factor has a direct impact on the compactness, microstructure and mechanical properties of the final part.

1.2 Overview of aluminum matrix composites

Metal matrix composites (MMCs) consist of two or more different phases that are distributed in an appropriate form to obtain properties that their single phase does not have. Typically, metal matrix composites consist of a metal or alloy as the matrix phase and cermet or metal-containing intermediate phase as the reinforcing phase. Among them, aluminum metal matrix composites (MMCs) have a wide range of application prospects in the aerospace and automotive industries due to their good wear resistance, high specific strength and low thermal expansion coefficient [6].

1.2.1 Selection of matrix materials

There are many types of aluminum alloy materials, and the common systems used in SLM forming are Al-Cu-Mg, Al-Mg-Sc- (Zr), Al-Zn-Mg, Al-Si, etc. In SLM forming applications, the main problems of aluminum alloy materials are poor powder fluidity, high thermal conductivity, easy oxidation, and low laser absorption. Compared with high-strength aluminum alloy systems, the alloying elements of aluminum alloy systems with high Si content have better fluidity in the molten state, which is conducive to reducing defects such as microcracks. Compared with other aluminum alloy systems (such as Al-Cu-Mg, Al-Zn-Mg, etc.), AlSi10Mg has better casting and welding performance, so the SLM

forming ability is better [7]. Therefore, AlSi10Mg was selected as the matrix material for this study.

1.2.2 Selection of enhanced phases

The selection of reinforcing phase particles usually considers properties such as modulus of elasticity, thermal stability, strength, and wear resistance. Therefore, oxides, carbides, nitrides and borides have become the most common aluminum alloy reinforcing phases. TiB2 itself has the advantages of high elastic modulus, high hardness and good thermal stability. Moreover, TiB_2 and Al have good lattice matching and interface binding ability[8]; In addition, TiB_2 can be used as a heteronuclear agent for aluminum alloys, promoting the refinement of Al grains and improving the mechanical properties of composite materials. Therefore, TiB_2 was selected as the reinforcing phase material for this study.

1.3 Research status of SLM formed aluminum alloy and its composite materials

With the rapid development of 3D printing technology and a wide range of fields, and the research and development of equipment is also quite mature, most scholars at home and abroad have carried out research on all aspects of aluminum alloy powder SLM forming [9], but the research on the surface roughness of aluminum alloy SLM forming parts is not enough, especially the dimensional accuracy of aluminum alloy SLM forming parts.

J.P. Kruth, Ben Vandenbroucke et al. [10,11] studied the influence of dimensional accuracy of biocompatible metal SLM forming specimens, and the results showed that appropriate changes in the influencing parameters such as spot diameter can effectively improve the dimensional accuracy of the specimen.

Yang Xiongwen [12] studied the dimensional accuracy of 316 stainless steel powder SLM forming parts, and the results showed that the sources of SLM forming dimensional error mainly included pre-data processing, SLM forming process and post-processing; The

dimensional accuracy decreases with the increase of laser power and energy density, and increases with the increase of scanning speed and scanning spacing. The scanning strategy is the best to reduce the dimensional accuracy of S-shaped orthogonal layer staggered forming, and the relationship between spot compensation, scanning error and energy density is established, which can improve the dimensional accuracy of SLM molded parts, and the dimensional accuracy of assembled parts after forming is ±0.1 mm.

Spierings A.B. et al. [13] studied the effect of particle size distribution of AM steel powder on SLM forming quality, and the results showed that the powder particle size had a great influence on surface roughness, and the optimized metal powder could form better parts.

Qian Kun [14] et al. analyzed the molding situation of SLM molding structure with gap under different placement methods. The placement methods are mainly divided into three types: horizontal placement, vertical placement and oblique placement. Each process parameter has an impact on the surface quality, the surface roughness of the molded part gradually decreases with the increase of laser power, with the increase of scanning spacing and scanning speed shows a trend of first decreasing and then increasing, the optimal parameter combination is scanning spacing 0.08 mm, laser power 200 W, scanning speed 600 mm/s. The surface roughness gradually increases with the increase of the inclination angle, and the tilt angle has a greater influence on the surface roughness of the overhanging structure, when the bulk energy density is 80 J/mm~3 to 110 J/mm~3, the upper and lower surface quality of the molded parts are the best.

Zhang Luo [15] et al. established a theoretical model of horizontal dimensional error and sharp angle error of straight plate and inclined plate according to the bottom-up additive manufacturing characteristics of SLM forming line-surface-body. It is found that the dimensional error in the X/Y direction of the straight plate structure is composed of two parts: melt channel width and cooling shrinkage. The melt width increases the forming size, and the cooling shrinkage reduces the forming size. When the X/Y size is small, such as the

thickness direction of the thin plate, the dimensional error mainly comes from the melt width. When the X/Y size is large, such as the length direction of the thin plate, its dimensional error is not only derived from the width of the melt channel, but also the cooling contraction can not be ignored, or even the main source. The dimensional error in the direction of the thickness of the inclined plate includes not only the width of the melt channel and the cooling shrinkage, but also the dimensional error caused by the overhang effect. The X/Y direction dimensional error model of the straight plate structure and the inclined plate structure are in good agreement with the actual measured value, and the difference between the two is within 20μm. For sharp corner structures without overhangs, the angle value after SLM forming is equal to the design value.

1.4 The main research content of this paper

In order to explore the optimal process parameters of the dimensional accuracy and surface roughness of the formed parts and the selective laser melting forming, the influence of the laser selective melting molding process parameters on the formed parts under different printing directions and the influence of TiB_2 nanoparticles on the dimensional accuracy and surface roughness of the formed parts. The main research contents of this paper are as follows:

1. Optimization of laser selective melting and forming process parameters of $AlSi_{10}Mg/TiB_2$ aluminum alloy powder

In view of the influence of different process parameters (laser power, scanning speed, powder thickness, etc.) on the dimensional accuracy and surface roughness of the formed parts by laser selective melting and forming, orthogonal experiments are first used to explore the process parameters that have the greatest influence on roughness and dimensional accuracy, and the best process parameters for dimensional accuracy and surface roughness of formed parts are found.

2. The influence of the printing direction of the formed part on the dimensional accuracy and surface roughness

After obtaining the best forming process parameters, explore the different printing directions (horizontal, height, inclination) of the molded parts, the influence on the surface dimensional accuracy and surface roughness of the molded parts, and find out the best printing direction of the molded parts.

PART 2. EXPERIMENTAL MATERIALS, EQUIPMENT AND TEST METHODS

This chapter mainly introduces experimental materials, SLM forming equipment, technical routes, experimental preparation, test characterization and experimental methods.

2.1 Experimental materials

The powder material used in the experiment of this paper is $AlSi_{10}Mg$ powder produced by German TLS company, with a particle size distribution range of 15 μm -50 μm, an average particle size of 30 μm, and the surface morphology and chemical composition of the powder are shown in fig. 2.1 and table 2.1, respectively. It can be seen from fig. 2.1 that the surface morphology of $AlSi_{10}Mg$ powder is basically spherical, accompanied by a small amount of spherical satellite powder attached to the surface of large spherical powder.

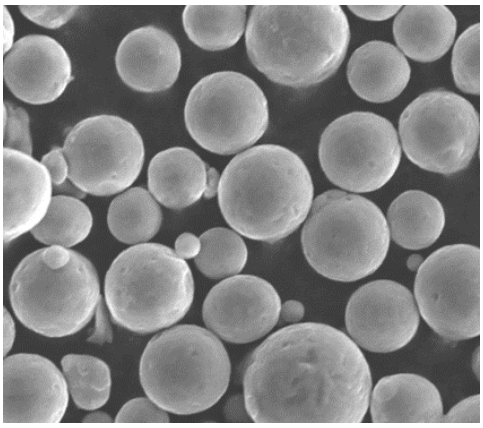

Fig. 2.1. Surface morphology of $AlSi_{10}Mg$ powder.

Table 2.1

AlSi10Mg powder main component composition

AlSi10Mg	The main elements			Impurities, not greater than					
	Al	Si	Mg	Fe	Cu	Mn	Ti	Zn	O
Wt%	Balance	9.0-11.0	0.2-0.45	0.55	0.05	0.45	0.15	0.10	0.10

2.2 Experimental equipment

2.2.1 Select laser melting equipment

In this experiment, the BLT-S210 selective laser melting equipment developed by Xi'an Bolite was used to prepare $AlSi_{10}Mg/TiB_2$ samples, and the schematic diagram is shown in fig. 2.2 (b).

BLT-S210 selective laser melting equipment working system mainly includes optical component system, intelligent mechanical system, motion forming system, circulation purification system and atmosphere protection system, etc., the equipment is equipped with IPG fiber laser, the laser can produce a maximum laser power of 500 W, and the use of F-θ lens, beam quality M2<1.1, the main performance parameters are shown in table 2.2. The equipment is capable of stable operation and has a wide range of adjustable process windows, meeting all the requirements required for testing in this paper.

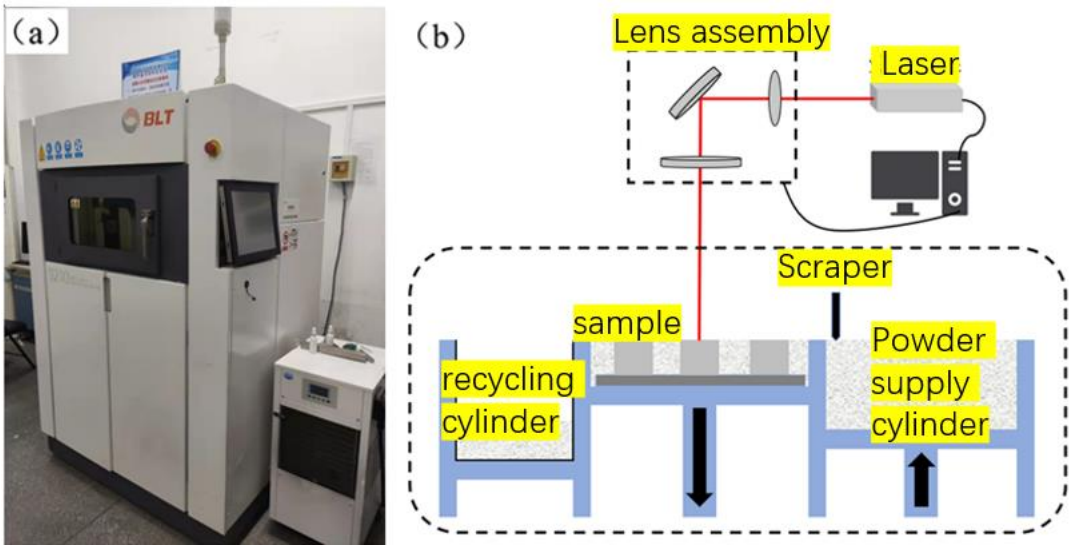

Fig. 2.2. Experimental equipment: (a) Forming equipment diagram; (b) Forming schematics.

Before the SLM forms the specimen, the following work is required:

(1) In order to ensure that the powder has good fluidity, use DZF-6090 vacuum drying oven to dry the moisture in the powder, heat it at 110 °C, and keep it warm for 5 hours;

(2) According to the experimental needs, use the supporting Build Process processing processor software to set the various process parameters required for the test;

(3) Use Magics 24.0 3D software to draw a three-dimensional model of the parts, establish a reasonable support structure with a height of about 2 mm at the bottom, match the process parameters in the BP processing processor software, and discretize them into a certain thickness and sequential slice file (generally STL format file);

Table 2.2

Basic parameters of BLT-S210 equipment

Technical indicators	Parameter
Laser wavelength	1060-1080 nm
Maximum laser power	500 W
Maximum scanning speed	7000 mm/s
Laser spot diameter	60 μm
Layer thickness	20-100 μm
Preheating temperature	≤200 ℃
Oxygen content in the forming chamber	≤100 ppm
Forming size (W×D×H)	105×105×200 mm（Does not include substrate dimensions）

The aluminum alloy substrates selected in this study are 105×105×20 mm, and the selected scraper is a steel scraper, which is wiped clean with alcohol and the scraper before installation. After installing and adjusting the plane of the substrate, the first layer of pre-coating powder is carried out, and the argon gas replacement of the forming cavity is carried out after the pre-coating is completed. When the oxygen content in the forming chamber is below 1000 ppm, turn on the fan, preheat the substrate to the experimental set temperature, and reduce the oxygen content in the forming chamber to less than 100 ppm before the forming experiment begins. fig. 2.3 shows the printing process diagram and the drawing of

some parameter forming specimens. After the specimen is formed, the specimen is separated from the substrate from the support using a wire EDM machine of type DK7355.

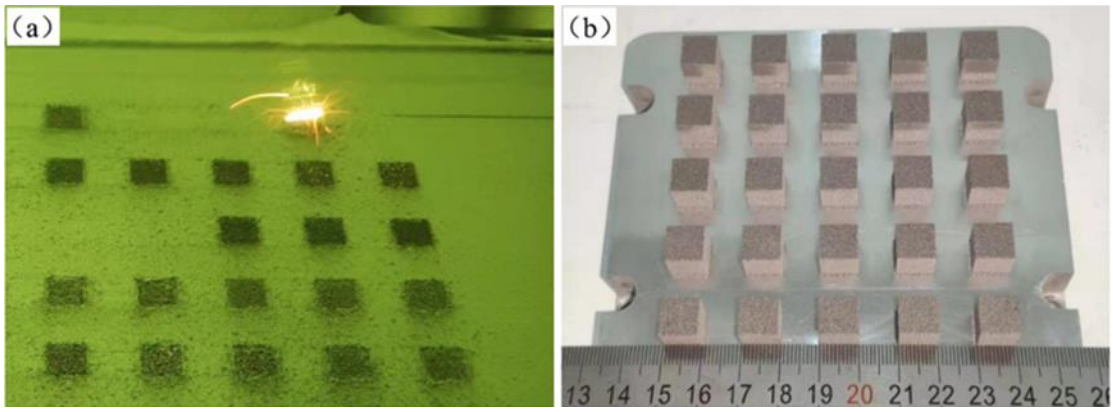

Fig. 2.3. Part of the parameter forming diagram: (a) printing process; (b) Forming the specimen.

2.2.2 Low energy ball milling equipment

The XQM-2 vertical planetary mill was used to mechanically mix $AlSi_{10}Mg$ powder and nano-TiB2 powder. The planetary mill is mainly composed of a motor device, a planetary structure, a ball mill and other structures, and the maximum rotation speed of the motor-driven mill is 670 rpm. When setting the ball milling parameters, it should be considered whether alloying or deformation of raw materials will occur between raw materials, so it is necessary to set suitable ball milling parameters so that different types of powders can be mixed evenly, and the combination between different powders can be more reliable and not easy to fall off. The low-energy ball milling device and schematic diagram are shown in fig. 2.3.

The main process of composite powder preparation is as follows:

(1) $AlSi_{10}Mg$ alloy powder, TiB_2 powder and stainless steel grinding balls of different sizes are added to the ball mill tank according to the proportion, and the ball-to-material ratio is set to 1:1;

Figure 2.4. Low-energy ball mill: (a) low-energy ball milling equipment; (b) Schematic diagram.

(2) Slowly fill the argon into the ball mill tank to prevent the argon pressure from flying out of the powder, and seal the ball mill tank after replacement to prevent powder oxidation;

(3) Set the appropriate ball milling parameters, as well as the appropriate ball milling method to prevent the temperature of the ball mill tank from being too high, therefore, set the ball milling mode of rotating for 30min, stopping for 5min, and then rotating in reverse after each stop;

(4) After the ball milling program is completed, wait for the ball milling tank to cool down and then open the ball milling tank, and use a mesh screen slightly smaller than the grinding ball particle size to separate the grinding ball from the powder.

2.3 Material performance test methods and characterization

2.3.1 Experimental methods

Since the factors affecting experimental performance include laser power, solid scanning speed, contour scanning speed and scanning spacing, there are many influencing

factors, and it is difficult to find out the main influencing factors in the early stage, so orthogonal experiments are used to explore the influence degree of each influencing factor.

First, select the appropriate orthogonal table, and then carry out experiments according to the orthogonal experimental table, and finally analyze the experimental measurement results, the density, hardness, dimensional accuracy and surface roughness of AlSi10Mg aluminum alloy SLM molded parts are the results of the comprehensive action of forming equipment, forming materials, forming parameters and other factors. When designing the experiment, the influence of laser power P, scanning speed V, scanning distance S and other parameters on them is mainly considered.

Table 2.3

Impact factors and levels

Process parameters	Laser power（W）	Entity scan speed（mm/s）	Contour scan speed（mm/s）	Scan spacing（mm）
Level 1	230	1100	700	0.15
Level 2	290	1300	900	0.17
Level 3	350	1500	1100	0.19

Table 2.4

Specific process parameter table

Process parameters	Laser power (W)	Entity scan speed (mm/s)	Contour scan speed（mm/s）	Scan spacing（mm）
1	230	1100	700.00	0.15
2	230	1300	900.00	0.17
3	230	1500	1100.00	0.19
4	290	1100	900.00	0.19
5	290	1300	1100.00	0.15
6	290	1500	700.00	0.17
7	350	1100	1100.00	0.17
8	350	1300	700.00	0.19

9	350	1500	900.00	0.15

2.3.2 Density analysis

The relative density of SLM-shaped specimens is measured using an STP JA1003 precision electronic balance (accuracy: 0.0001 g) based on the Archimedes principle. Due to the presence of a little sticky powder on the surface of the formed specimen, the surface of the specimen is sanded before weighing, cleaned and dried with an ultrasonic cleaning machine. Each formed specimen is weighed three times and the average is taken as its relative density value, and the calculation formula is:

$$\rho_1 = \frac{m_1 \rho_0}{m_1 - m_2} \tag{2-1}$$

$$\rho_2 = \rho_{\mathrm{AlSi10Mg}} \times \omega_1 + \rho_{TiB_2} \times \omega_2 \tag{2-2}$$

$$\eta = \frac{\rho_1}{\rho_2} \times 100\ \% \tag{2-3}$$

Where: ρ_0: the density of deionized water, the density of ionized water at room temperature (20 °C) is ρ_0 is 0.998203 g/cm^3; ρ_1: the actual density of SLM forming specimens (g/cm^3); m_1: the mass of the sample in air (g); m_2: mass of the sample in deionized water (g); ρ_2: the theoretical density of SLM forming specimens (g/cm^3); ρ_{AlSi10Mg}: theoretical density of $AlSi_{10}Mg$ aluminum alloy (g/cm^3); ω_1: the mass fraction of $AlSi_{10}Mg$ aluminum alloy in the sample; $\rho_{(TiB2)}$: theoretical density of TiB_2 (g/cm^3); ω_2: The mass fraction of TiB_2 in the sample. The relative density of SLM shaped specimens is measured using the above method.

2.3.3 Test characterization of surface roughness

When AlSi10mg aluminum alloy powder is formed in SLM, due to the light weight and easy oxidation of the aluminum alloy powder itself, it is easy to produce splashing of molten liquid under the irradiation of the laser beam and accompanied by nodularization, resulting in poor quality of the upper surface (X-Y side) of the molded part, so this paper mainly studies the surface roughness of the Y-Z surface on the left side of the molded part

(as shown in fig. 2.7). In this paper, JB-6C contour roughness tester is used to measure the maximum height of the contour on the outer surface Ra.

The specific steps are, first install the measuring probe to the measuring beam, and then fix the sample on the stage, operate the button to make the probe and the measurement surface in close contact, meet the measurement requirements, set the measurement parameters and measurement requirements, and then click the "Start Measurement" button on the computer to carry out automatic measurement, read the experimental measurement data, mainly from the surface roughness Ra value change to analyze, and then use a super-depth three-dimensional microscope to analyze the outer surface contour of the sample.

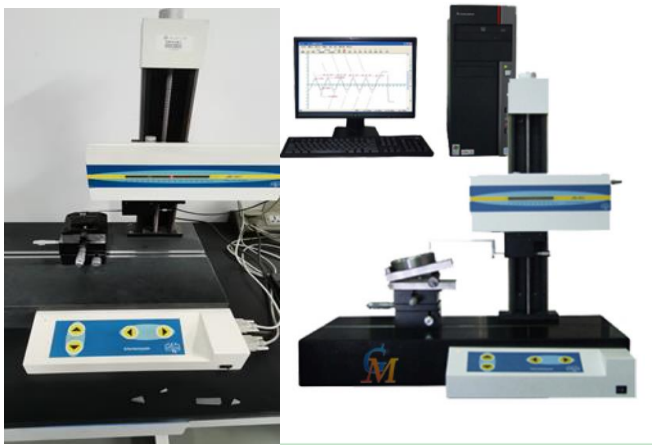

Fig. 2.6. JB-6C contour roughness tester.

2.3.4 Measurement characterization of dimensional accuracy

The dimensional accuracy of this paper is expressed by the deviation value between the actual measured size in different directions and the experimental design size, that is, the size of the standard part, the larger the dimensional deviation value, the lower the forming accuracy, and vice versa. The dimensions in the Z direction of SLM molded parts will produce large errors due to wire cutting treatment, etc., so this article only studies the dimensional accuracy in the X and Y directions, and fig. 2.7 is the dimensional pattern of the formed parts.

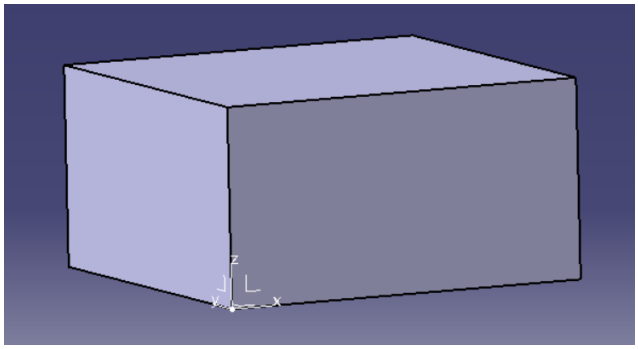

Fig. 2.7. Dimensional pattern of formed parts.

Through the test tool micrometer to measure the size in the X and Y directions, in order to minimize the manual error measurement, the size of different positions is measured many times, the data with a large gap is excluded, and finally three valid data are measured, and the average value of the three data is taken as the actual size measurement value.

PART 3. INFLUENCE OF PROCESS PARAMETERS AND FORMING POSITION ON THE DIMENSIONAL ACCURACY AND SURFACE ROUGHNESS OF SLM FORMING ALSI10MG/TIB_2 ALLOY

Through preliminary experiments, it is found that the use of powders with different uses has a serious impact on the surface roughness and dimensional accuracy of the molded parts. Fig. 3.1 shows a comparison chart of the side surface topography of the molded part, and fig. 3.2 shows the comparison chart of the upper surface topography of the molded part.

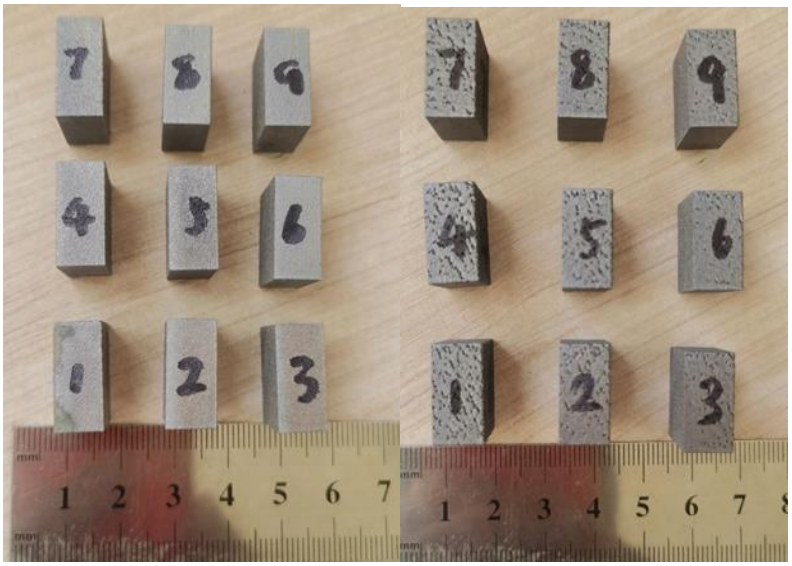

Fig. 3.1. Comparison chart of the side surface topography of the formed part.

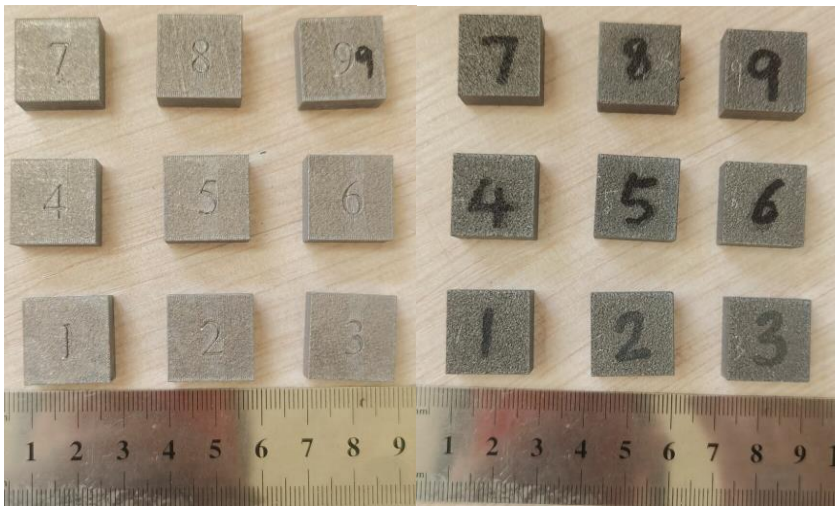

Fig. 3.2. Comparison chart of the upper surface topography of the molded part.

It can be seen from the figure that the powder with different uses has a greater influence on the SLM forming sample, the surface of the unused powder SLM molded parts is smoother and the metal color is better, and the recycled powder SLM molded parts with more use times have more holes on the surface and the metal color is poor. The following will analyze the impact from several aspects, such as the change of powder particle size distribution, the change of powder accumulation characteristics, the change of powder morphology, the oxide on the surface of the powder, and the evolution mechanism of the powder particles.

3.1 Effect of AlSi10Mg alloy powder on SLM molding

3.1.1 Changes in powder particle size distribution

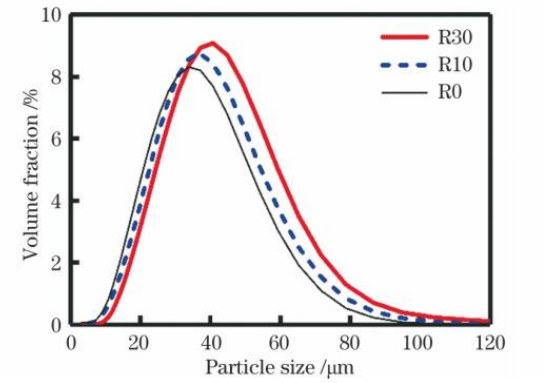

Fig. 3.3. Particle size distribution of AlSi10Mg powder recycled powder.

The variation law of the particle size of the recycled powder is shown in Figure 3-3. For powders that are recycled 10 and 30 times, the differential distribution curve of the particle size is clearly shifted to the right and the particle size is more concentrated (relative to the initial powder), a trend that indicates a coarsening of the powder particles, i.e. a decrease in the proportion of smaller powders and an increase in the proportion of larger powders. D10, D50, D90 (D10, D50, D90 refer to the percentage of powder diameter less than a certain value of 10%, 50% and 90%, respectively). The D90 of the powder used for 10 and 30 cycles was 5.75% and 14.5% larger than that of the initial powder, and D10 was

increased by 9.7% and 26.5%, respectively, which further indicated that the particle size of the powder increased with the increase of the number of cycles. D50 increased from 30μm of the initial powder to 35.5 μm after 30 cycles, and the proportion of the circulating powder size in the range of 30-35.5 μm was higher than that of the initial powder, indicating that the particle size of the recycled powder was more concentrated. The results of this paper are consistent with the results of Heiden et al. and Tang et al., indicating that the particle size of the powder will be severely coarsened and the particle size will be more concentrated during the powder recycling process.

The analysis believes that there are three reasons for this phenomenon: first, in the SLM process, the spread of the powder is achieved by the powder scraper, because the smaller size of the powder has the effect of filling the gap of the large size of the powder, coupled with the percolation effect of the powder of different particle sizes, so the fine powder is easy to be deposited in the lower part of the accumulated powder layer during the powder laying process, and preferentially deposited to the upper surface of the formed layer; As the number of powder cycles increases, smaller powders are preferentially depleted and the proportion decreases. Second, in the process of laser-molten pool-metal vapor interaction, the metal vapor [17-18] is violently sprayed upward at the highest surface temperature of the molten pool, under the action of metal vapor dragging force, the argon around the molten pool forms a vortex, and the vortex produces horizontal dragging force on the freely accumulated powder around the molten pool, and the smaller size powder has a smaller dragging force and a large acceleration, and moves rapidly towards the molten pool/metal vapor at a higher horizontal movement speed; When these fine powders move to the molten pool/metal vapor, they will be sucked into the molten pool or ejected by the upward metal vapor, forming high-speed flying splash particles [18-19]; Coupled with the action of the transverse argon gas flow inside the forming chamber, splash particles can easily collect at the outlet of the argon gas flow or enter the circulation system, eventually resulting in a reduction of fine powder on the powder bed. Third, small-size powders have

a large specific surface area, and the total energy absorbed by complete melting is low, which can absorb more energy under the same laser parameters, resulting in excessive temperatures inside the molten pool [20], and small-sized powder particles can also be melted under heat conduction [21]. In addition, the small-sized powder particles near the molten pool are easily dragged into the molten pool under the action of the surface tension of the molten pool, and the size of the molten pool is increased after melting [20]. Under the combined action of laser radiation, heat conduction, vapor jet and laser plume, small-size powders will be preferentially consumed, and the main reason for the increase in the proportion of large-size powders is that large-size splashes will be generated during the laser-powder-molten pool-plume interaction, such as agglomeration particles, spherical particles, irregular particles, etc. Although the powder analyzed and tested in this test is strictly screened and dried, when the length-to-diameter ratio of the splash particles is different, some of them cannot be separated by the mesh screen, so that they are mixed into the circulating powder, which eventually leads to an increase in the proportion of large-size powder.

3.1.2 Changes in powder accumulation characteristics

Powder build-up characteristics such as bulk density, tapped density and flowability have a significant impact on the quality of SLM molded parts. The bulk density and tapped density affect the stacked arrangement of the powder on the upper surface of the substrate/formed layer, i.e. the density of the thin layer of the powder. Powders with high bulk density and tapped density can obtain a relatively dense powder thin layer after powder coating, reduce the void between powder particles, and form a continuous, nopheric defect-free melt channel under suitable laser processing parameters [20,22]. Fluidity refers to the time required for a certain amount of powder to flow continuously through a certain pore size, reflecting the dynamic rheological characteristics of the accumulated powder, and is a comprehensive reflection of the powder shape, surface state, particle size distribution and

other indicators. Powders with good fluidity have good spreading properties, which is conducive to the formation of dense powder thin layers. However, the flow time is not as short as possible, because the fluidity is greatly affected by the particle size distribution, and the large-sized powder particle group has good fluidity, but at the same time, it also has a large size of the void, and cannot form a dense powder thin layer. Therefore, indicators such as particle size distribution, bulk density, tapped density, and flowability must be considered comprehensively.

With the increase of the number of powder cycles, the loose density and tapped density of the powder decrease to a certain extent, but the fluidity of the powder increases (the time for the powder to flow through the Hall flow meter decreases). The bulk density, tapped density and fluidity of the powder are related to the particle size distribution, surface roughness, humidity and other factors, and are closely related to the dynamic rheological properties of the powder (the dynamic rheological properties directly affect the spreading behavior of the accumulated powder on the upper surface of the powder bed/formed layer). Changes in powder particle size, especially a decrease in the proportion of fine powders, reduce the van der Waals force between powder particles and weaken bridging, thereby improving the fluidity of recycled powders. However, the larger size of irregular particles will make the accumulated powder have more voids and bridging phenomenon, which will reduce the bulk density and tapped density of the accumulated powder. The experimental results of this paper also show that the reasonable combination of powders of different particle sizes, that is, the use of spherical metal powder as much as possible, without affecting the fluidity of the powder, adding a certain proportion of fine powder to fill the void formed by the coarse powder can improve the loose density and tapped density of the powder, thereby improving the density of the thin layer of powder on the powder bed.

3.1.3 Changes in powder morphology

In the SLM process, the laser-powder-molten pool-plume interaction causes a large change in the surface morphology of the unmelted powder particles in the forming chamber. Figure 3 shows the macrosurface topography of the initial powder and the recycled powder. As can be seen from fig. 3.4 (a), the initial powder is mostly spherical and contains only a small amount of satellite spheres, which is an inherent property of true air atomized powders. With the increase of the number of cycles, in addition to containing a small amount of satellite spheres, the powder also contains a large number of large-size particles, irregular particles, rod-like particles and broken particles, as shown in the circle, square and rectangular box in fig. 3.4 (b), (c) (different figures represent different types of powder particles). Comparing fig. 3.4 (a), (b), and (c), it can be found that there are almost no small-sized powder particles in the powder after 30 cycles, which is consistent with the decrease in the proportion of small-sized powders in the particle size distribution analysis of section 3.1.1. The recycled powder contains larger particles with a smooth surface (as shown by the dotted circle in fig. 3.4), which are produced by laser-induced sputtering of the molten pool, which is similar to the gas atomization process (discussed in Section 3.1.5), or the surface of the powder particles undergoes rapid surface heat treatment by laser heating, resulting in surface modification. As the number of cycles increases, black spots appear on the surface of the large-sized powder particles, that is, oxides are formed, as shown in the dotted circle in fig. 3.4 (c).

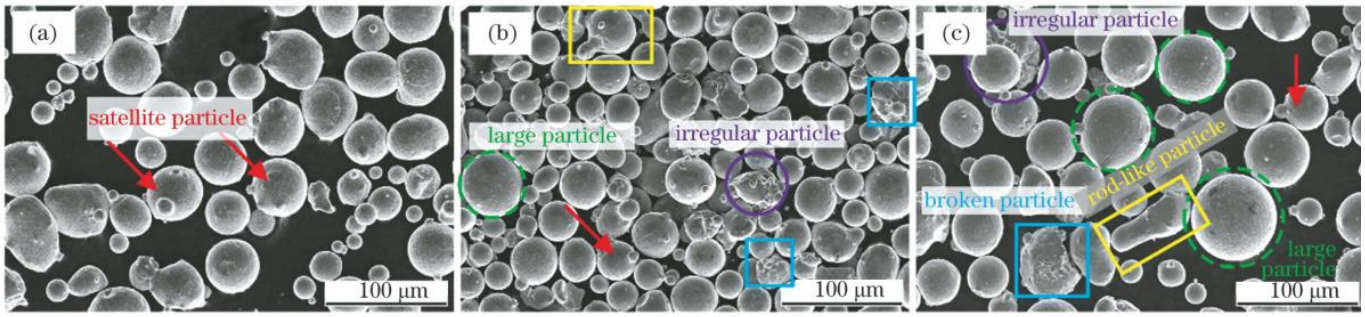

Fig. 3.4. Surface morphology of AlSi10Mg powder recycled powder. (a) initial powder; (b) 10 cycles; (c) Cycle 30 times.

3.1.4 Oxides on the surface of the powder

Fig. 3.6 shows the EDS spectrum of powder particles with round black spots on the surface after 30 cycles. As can be seen from the figure, the diameter of the powder particles with black spots is greater than 50 μm, and it is inferred that these large-sized particles are additional products produced during SLM. In fig. 3.5, no particles with black spots were found in the initial powder and the powder that was recycled 10 times. The diameter of the round black spot was measured using Image J software, and the diameter distribution range was 3.2~16.1 μm.

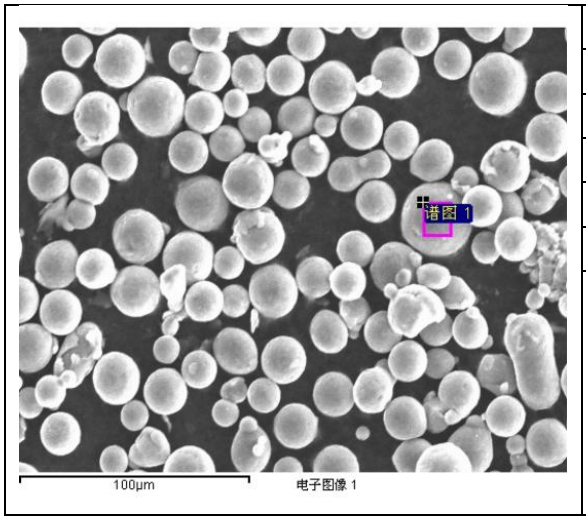

Elements	Weight%	Atom%
O	0.92	1.54
Mg	0.24	0.27
Al	86.73	86.60
Si	12.06	11.56
Fe	0.06	0.03
Total	100	100

Fig. 3.5. New powders element content.

EDS spot scanning was performed on the surface of the powder particles and their adjacent areas, and the element content was qualitatively analyzed, and the scanning results were shown in fig. 3.7. It can be seen from the EDS spectrum that the black spots are rich in Si and O elements, and also contain Fe and Mg elements. The element content of black spots is shown in fig. 3.6, it can be seen that black spots are enriched in Si and O elements, and the content of Fe is much lower than that of $AlSi_{10}Mg$ initial powder, and the O element content is hundreds of times that of the initial powder. From EDS qualitative and

quantitative analysis, it can be seen that the black spots are oxides of Si and Al. It can also be seen from the figure that bands of oxides appear between oxidation spots and the phenomenon that spots are connected to spots. This indicates that after multiple cycles of the powder, the oxide spots rich in Si and Mg may be connected to each other to form a layer of oxide film on the surface of the powder particles.

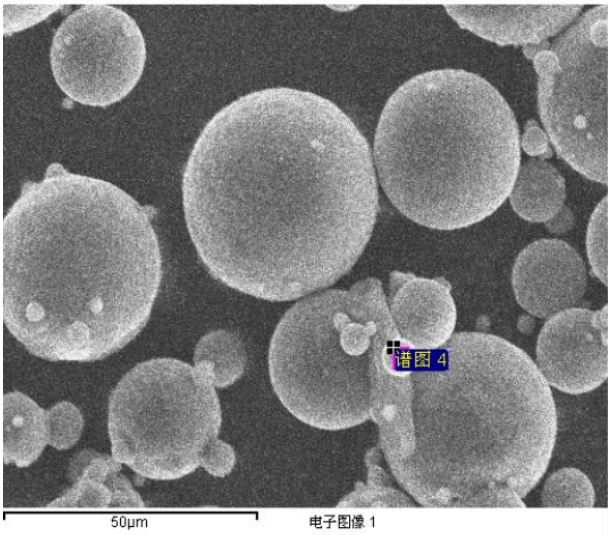

Elements	Weight%	Atom%
O	19.93	29.71
Mg	0.43	0.43
Al	72.70	64.27
Si	6.24	5.30
Fe	0.69	0.30
Total	100	100

Fig. 3.6. Old powders element content.

The formation mechanism of circular oxidation spots is as follows: laser-powder interaction produces a high-temperature liquid molten pool, and the mesoscopic molten pool has a high temperature gradient, which will produce violent Marangoni convection, making the molten pool sharply unstable; The lateral flow of gases around the molten pool caused by the Bernoulli effect and the protective gas flow (argon) further increase the instability of the micro-molten pool; The unstable high-temperature liquid molten pool produces liquid droplet splashing under the action of vapor recoil pressure, and the droplet splash may oxidize during flight. AlSi10Mg powder contains volatile elements Mg, Si, and Si and Mg elements have a strong affinity for O elements, and the rate of diffusion of Si and Mg

elements to the surface of particles is relatively fast during the flight of high-temperature droplet splashes, which further increases the possibility of forming oxide spots on the surface of high-temperature splash particles.

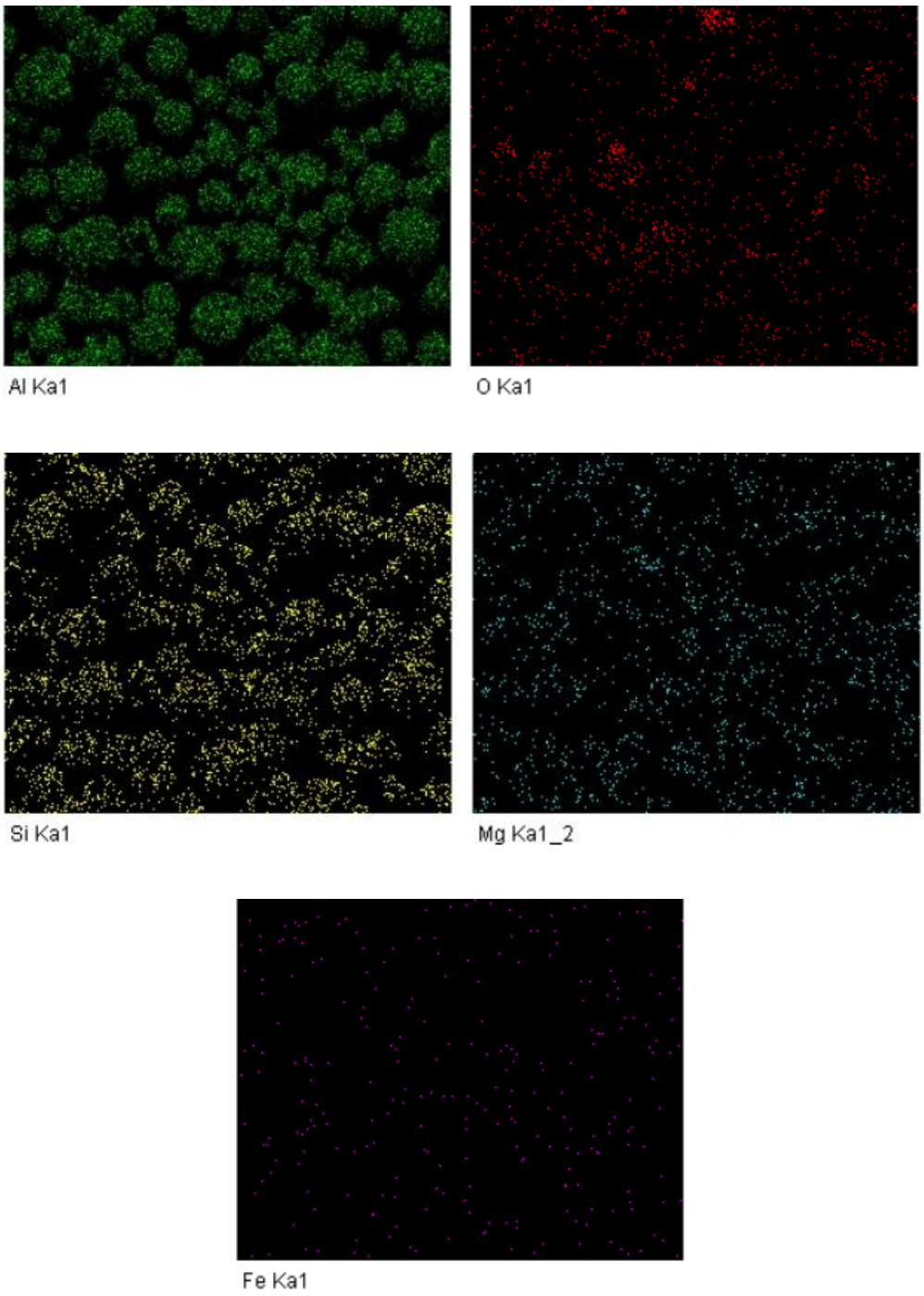

Fig. 3.7. EDS results of circular black spots on the surface of powder particles are recycled 30 times.

In addition, according to Ellingham diagram [26], the oxidation potential energy of Mg and Si is much lower than that of Fe, although the volume fraction of oxygen in the forming chamber is controlled below 5×10^{-4}, but Mg and Si elements still have high local partial pressure of oxygen, so AlSi10Mg can still oxidize inside the forming chamber, resulting in the formation of oxidation spots of Mg and Si on the surface of the flying high-temperature sputtering particles. The shape of the oxidized spot is round, because the circle has the least surface energy, which is more conducive to the nucleation and growth of the oxidized spot.

Morrow et al. [27] and Schaller et al. [28] found a large number of nanometer-sized Mg and Si oxides at the grain boundaries of the molten molded parts of the laser powder bed, and Heiden et al. and Zhao et al. [29] also found that the formation of oxides is detrimental to the mechanical properties of the molded parts. Li Ruidi [30] found similar oxide spots on the surface of the molded parts and pointed out that the increase in oxygen content in the powder is not conducive to the forming process and produces nodularization defects. The increase of oxide on the surface of powder particles will increase the oxygen content in the molten pool, thereby further changing the wetting behavior of the high-temperature molten pool [30] and the surface tension temperature coefficient of the high-temperature molten pool [31], changing the flow direction of the melt [31-32], and then promoting the formation of defects such as pores, unfused, and cracks inside the molded parts.

3.1.5 Evolution mechanism of powder particles

The SLM process is a multi-scale process in which the microscopic scale (formation of microscopic structure) – mesoscopic scale (powder melting to form a molten pool) - macroscopic scale (mechanical properties) are coupled with each other, and various physical, chemical, metallurgical and other reactions occur . In order to distinguish the morphology of powder particles, this paper divides the particles into two categories according to the

formation mechanism of special-shaped particles, the first is laser-induced molten pool sputtering particles, and the second is gas entrainment-induced special-shaped particles. Laser-induced formation mechanism of sputtered particles in molten pool: In the process of laser interaction with powder particles to form molten pool, the high energy density laser heats the powder containing metal elements with low melting point, generating a large amount of metal vapor above the molten pool and a strong downward recoil pressure.

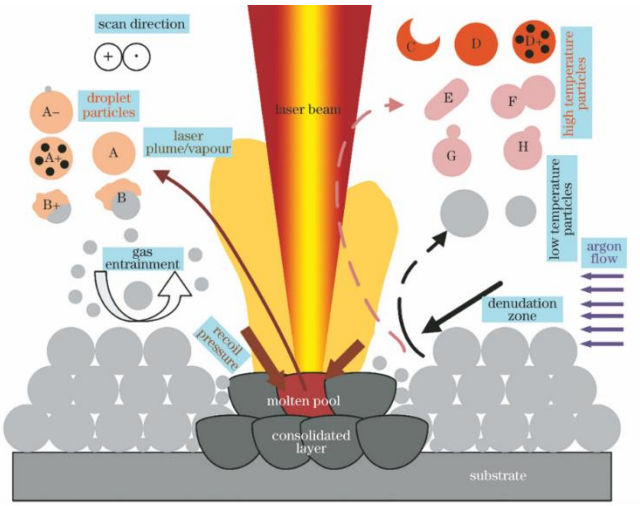

Fig. 3.8. Schematic diagram of laser-powder-molten pool interaction.

At the same time, the extremely high temperature gradient inside the high-temperature molten pool produces strong Marangoni convection flowing radially outward. Under the combined action of surface tension, recoil pressure and Marangoni convection, the high-temperature liquid molten pool is in equilibrium and stable state. When Marangoni convection and recoil pressure exert more drag force on the high-temperature melt than the surface tension, it will promote the instability of the high-temperature liquid molten pool, and the molten material will sputter out of the high-temperature molten pool, forming sputtered high-temperature liquid droplets. The flying high-temperature liquid molten droplets form spherical particles of larger size under the action of surface tension, such as particle A shown in fig. 3.8, or particle shown in the dotted circle in fig. 3.4. After the high-

temperature molten droplets collide with larger cryogenic particles at a higher speed during flight, irregular particles B and B+ will be formed, as shown in the solid circle of fig. 3.4. A-particles are formed when high-temperature droplets collide with smaller cryogenic particles at a lower speed during flight. If the sputtered liquid droplet particles fall to the powder bed before solidification, they will adhere to the surrounding low-temperature powder particles, forming larger agglomerated particles. Due to the rigorous sieving of the circulating powder used in the test, no agglomerated particles of larger size were observed. Gas entrainment phenomenon induces the formation mechanism of special-shaped particles: in the process of laser-powder interaction, a liquid molten pool will be produced in a very short time, and when the surface temperature of the molten pool is high enough to reach the boiling point of $AlSi_{10}Mg$ powder, evaporation will occur, and the evaporation degree is the most intense where the surface temperature of the molten pool is the highest, and strong metal vapor will be produced; When the upward vapor pressure exceeds the pressure exerted by the environment around the molten pool, the metal vapor will burst to form a vapor jet. Vapor jet induces the horizontal pressure difference of the ambient gas around the molten pool, and it can be seen from the Bernoulli effect that the air flow around the molten pool will flow to the high-temperature molten pool, forming a laterally flowing argon air flow (the speed of the transverse argon gas flow is much smaller than the speed of upward injection of metal vapor [18-19]), this vapor-induced lateral air flow can drag the low-temperature powder particles around the molten pool to the molten pool, forming a phenomenon of vapor-induced lateral air flow entraining powder particles [19], The result is an area of ablation near the melt channel.

When the transverse argon gas stream entrains the powder particles into the area directly above the molten pool, the low-temperature powder particles will be heated and melted by the laser beam, metal vapor or laser plume [17], and will also be sputtered upward at a higher speed by the metal vapor/laser plume sprayed upwards at high speed, forming high-temperature sputtering particles, which can fly for a long time and a long distance in

the forming chamber. When the high-temperature sputtering particles are partially melted, broken particles C are formed, as shown in fig. 3.8, or as shown in the solid box in fig. 3.4. If the high-temperature splash is completely melted into small liquid droplets and does not collide with other particles during flight or before complete solidification, spherical particles of the same size as the initial powder will be formed under the action of surface tension; If the liquid droplets collide at high temperatures, they will merge and grow and form larger spherical particles D under the action of surface tension; If the temperature of particles A and D is high enough and the oxygen content inside the forming chamber is high, particles A + and D+ with circular oxide spots form on the surface of the particles. If the high temperature liquid molten droplets collide with other particles before completely solidifying, they will form rod-shaped particles E, sintered particles F, satellite sphere G or teardrop-shaped particles H. Although the probability of collision of high-temperature liquid droplets during flight is low, when the number of high-temperature liquid droplets in flight is sufficient, the possibility of collision will be greatly increased. The phenomenon of collision of SLM splash particles during flight has been studied by several scholars using high-speed X-ray imaging [19] or high-definition photography imaging. When the speed of the transverse argon gas flow entrained powder particles is low and cannot enter the high-speed and high-temperature vapor injection area above the molten pool, the powder particles will not be significantly heated, but the denudation area formed by the lateral movement of the powder will destroy the dense thin layer of powder accumulated on the powder bed, and when SLM is carried out in the next or next layer, discontinuous melting channels may be formed or defects such as non-fusion may be formed [20]. When the powder particles entrained by the transverse argon air flow located behind the molten pool move to the high-temperature molten pool, they may be sucked into the molten pool or semi-melted at the edge of the molten pool, affecting the continuity of the molten channel, and may eventually affect the uniformity of the next layer of powder laying or the quality of the formed parts [19]. When the argon gas stream carries particles to the upper surface of the melt channel

that has solidified but is in a high temperature state, it may adhere to the upper surface of the melt channel, which will also affect the uniformity of the next layer of powder.

3.2 Effect of process parameters on density of AlSi10Mg/TiB2 alloy formed by SLM

3.2.1 Orthogonal experimental results and analysis

According to the experimental requirements, the orthogonal experimental protocol was designed, and 9 samples of AlSi10Mg aluminum alloy were formed by SLM, all with dimensions of 18 mm(X)×18 mm(Y)×9 mm(Z). The density of the specimen is measured and the results are shown in the table. From the table, it can be seen that the best density is 99.5%, and the worst is 95.7%.

Table 3.1

Density orthogonal results

Experiment number	Density(%)	Experiment number	Density(%)	Experiment number	Density(%)
1	97.8	4	97.60	7	95.70
2	99.50	5	97.70	8	97.30
3	99.40	6	96.20	9	98.30

Table 3.2

Analysis of orthogonal experimental results

Serial number	Laser power	Entity scan speed	Scan spacing
Mean T_1	98.9	97.0	97.9
Mean T_2	97.2	98.2	97.1
Mean T_3	97.1	98	98.1
Range R	1.8	1.2	1.0

The mean density and range under the three factors were analyzed and calculated, and the results are shown in the table. It can be seen from the table that three factors have a certain influence on the density of the formed parts, among which the extreme difference R of the laser power is large, indicating that compared with the solid scanning speed and scanning distance, the laser power is the most important factor affecting the density of SLM forming parts.

3.2.2 Effect of laser power on density

In order to further explore the influence of laser power on the density of the sample, the scanning distance is 0.19 mm, the solid scanning speed is 1100 mm/s, 1300 mm/s, 1500 mm/s, and the laser power is 170 W, 200 W, 230 W, 260 W, 290 W, 320 W. The experimental results are shown in the fig. 3.9.

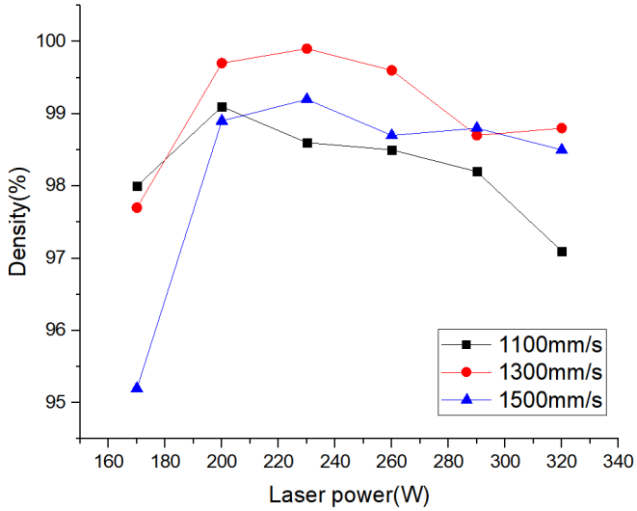

Fig. 3.9. Effect of laser power on relative density

The size of the laser power will directly affect the size of the molten pool, and defects such as spheroidization and holes will occur when it is too low or too high, resulting in a decrease in the density of the molded part. Laser power 170W, at this time the laser input energy is small, the powder may not be completely melted, and because SLM forming is

overlapping between the melt channel and the molten channel, the unmelted powder adheres to the molten channel around the phenomenon of different degrees of nodularization, which will not only affect the forming of the next layer of powder, but also lead to the formation of pores inside the molded part and become larger and larger, thereby reducing the density of the molded part. The laser power is 230 W, the laser input energy increases, the internal temperature of the molten pool increases, the width and depth of the melt channel will increase appropriately, at this time the powder melting is sufficient to reduce or inhibit the occurrence of nodularization, so that the density of the molded parts is improved. The laser power is 320 W, the density of the formed part does not rise but begins to decrease, the analysis reason may be because the input energy is too large, the width of the molten channel in the molten pool increases while the depth of the molten channel will continue to increase, the powder around the molten channel will adhere together, and too much energy will also cause the aluminum alloy molten liquid to splash during SLM forming, and then quickly solidify to form a granular form back to the surface of the formed part, so that the density of the formed part begins to decline. In summary, when the laser power is 230 W, the density of the formed part is the highest.

3.2.3 Effect of solid scanning speed on density

As mentioned earlier, SLM forming is a layer-by-layer process, a single deposition line is the basis of the entire process, by the single deposition line overlapping each other to complete the forming of each layer, so the main process parameter of each single layer forming is the scanning spacing. If the scanning distance is too large, and the lap between the single deposition lines is not enough, holes will appear at the lap joint, forming defects; The scanning distance is too small, although it is not easy to form defects such as holes in the lap area, but the remelting area will form coarse tissue, affecting the performance of the sample, and too much remelting will also affect the forming efficiency. Combined with the previous research, the laser power of 230 W, the layer thickness of 30 μm, the phase angle

of 67°, and the scanning spacing of 0.19 mm were selected, and the speed was 1100 mm/s, 1200 mm/s, 1300 mm/s, 1400 mm/s, and 1500 mm/s respectively.

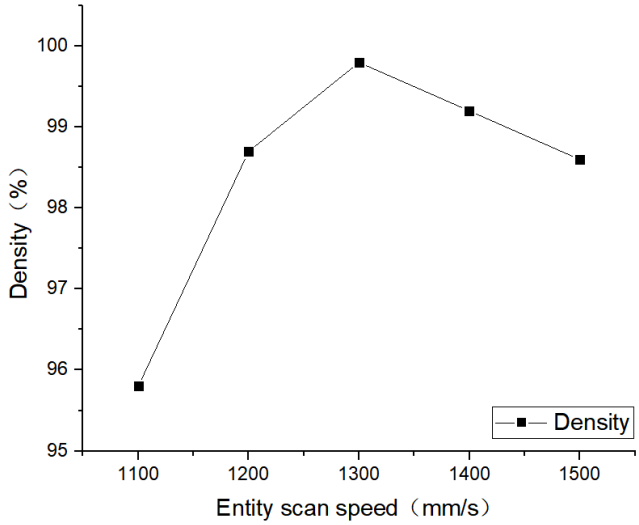

Fig. 3.10. Effect of solid scanning speed on density.

3.2.4 Influence of scan spacing on density

As mentioned earlier, SLM forming is a layer-by-layer process, a single deposition line is the basis of the entire process, by the single deposition line overlapping each other to complete the forming of each layer, so the main process parameter of each single layer forming is the scanning spacing. If the scanning distance is too large, and the lap between the single deposition lines is not enough, holes will appear at the lap joint, forming defects; The scanning distance is too small, although it is not easy to form defects such as holes in the lap area, but the remelting area will form coarse tissue, affecting the performance of the sample, and too much remelting will also affect the forming efficiency. Combined with the previous research, the laser power of 230 W, the layer thickness of 30 μ, the phase angle of 67°, the solid scanning speed of 1500 mm/s were selected, and the different scanning spacing parameters of 0.15 mm, 0.16 mm, 0.17 mm, 0.18 mm, and 0.19 mm were selected for comparative analysis.

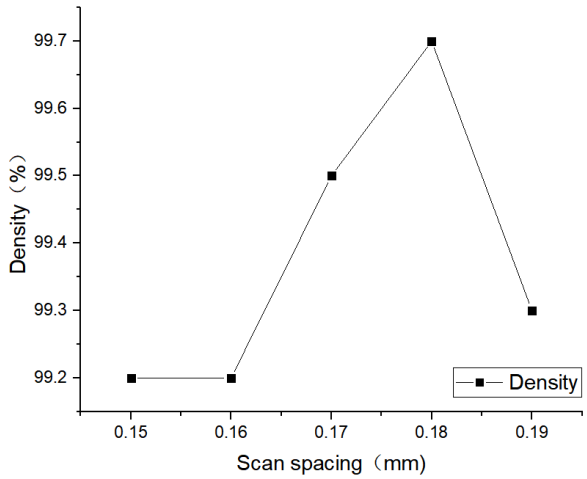

Fig. 3.11. Effect of scan spacing on density.

It can be seen from the figure that in the case of low scanning speed, the influence of scanning spacing on the density of formed specimens is not obvious, under the condition of scanning spacing of 0.15 mm and 0.16 mm, the relative density of the sample does not change much, while the relative density increases slightly when the scanning spacing is 0.17 mm, and the relative density reaches the maximum at 0.18 mm, which is 99.7%; When the scanning distance is 0.19 mm, the relative density begins to decline. The reason is that when the scanning speed is low, the laser energy density is larger, the molten pool exists for a longer time, so the single deposition line is wider, there is still a higher lap rate under a larger scanning spacing, the forming quality is better, and when the scanning speed is faster, the molten pool itself will become narrower, at this time, if the scanning spacing is too large, it is likely that there will be defects such as insufficient overlapping between adjacent deposition lines and the formation of holes, so the density of the sample will be reduced, as shown in fig. 3.12.

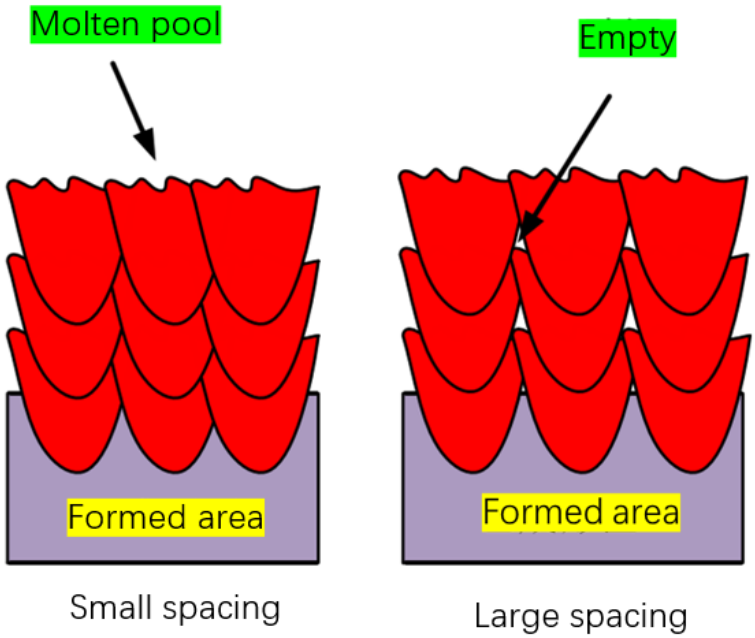

Fig. 3.12 Schematic diagram of different scan spacing forming.

3.3 Influence of process parameters on the dimensional accuracy of $AlSi_{10}Mg/TiB_2$ alloy formed by SLM

3.3.1 Influence of laser power on X/Y axis dimensional accuracy

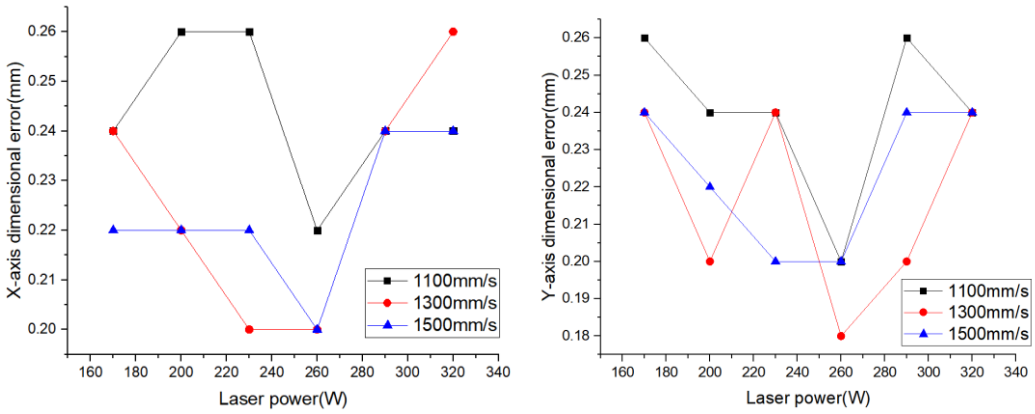

Fig. 3.13. Effect of laser power on X/Y axis dimensional error.

Fig. 3.13 shows the effect of laser power on the average dimensional error in the X and Y directions of $AlSi_{10}Mg$ aluminum alloy SLM molded parts. It can be seen from the figure that when the solid scanning speed is 1100 mm/s, the dimensional error in the X

direction increases with the increase of laser power, and when the laser power is 260 W, it decreases to 0.22 mm, and the dimensional error in the Y direction shows a trend of first decreasing and then increasing with the increase of laser power, and at 260 W, the minimum error is 0.20mm; When the solid scanning speed is 1300 mm/s, the dimensional error in the X axis direction is shown as a trend of increasing after decreasing, when the laser power is 260 W, the minimum value is 0.20 mm, the dimensional error in the Y axis direction shows irregular changes, and at 260 W, the minimum value appears 0.18 mm; At a solid scanning speed of 1500mm/s, the maximum dimensional error differs from the mean minimum dimensional error in the X direction by 0.04 mm, and the maximum dimensional error in the Y direction differs from the mean minimum dimensional error by 0.04 mm.

With the increase of laser power, the dimensional error in the Y direction is smaller than that in the X direction. The laser power is 260 W, and the dimensional error in the Y direction is smaller, but the difference is not large, because when the laser power is small, the input energy is small, the width and depth of the molten pool during forming are small, and the width of the formed molten channel becomes narrower, and even the powder cannot be continuously melted, so that the powder is not fully melted, so the final dimensional error is small; The laser power is 320 W, the dimensional error in the X and Y directions will become larger, due to the large energy input of the laser at this time, the powder melting is complete enough and the melting width becomes larger, which will cause some metal powder to adhere around the molten channel, making the dimensional error larger. In general, the laser power is too large or too small will make the dimensional error become larger, the laser power is 260 W, the corresponding $AlSi_{10}Mg$ aluminum alloy SLM forming parts density is also better, so when the laser power is 260 W, the X and Y dimensional errors will be relatively small, the average values are 0.200 mm and 0.18 mm, respectively, at this time the dimensional accuracy of $AlSi_{10}Mg$ aluminum alloy SLM forming parts is the highest.

3.3.2 Influence of solid scanning speed on X/Y axis dimensional accuracy

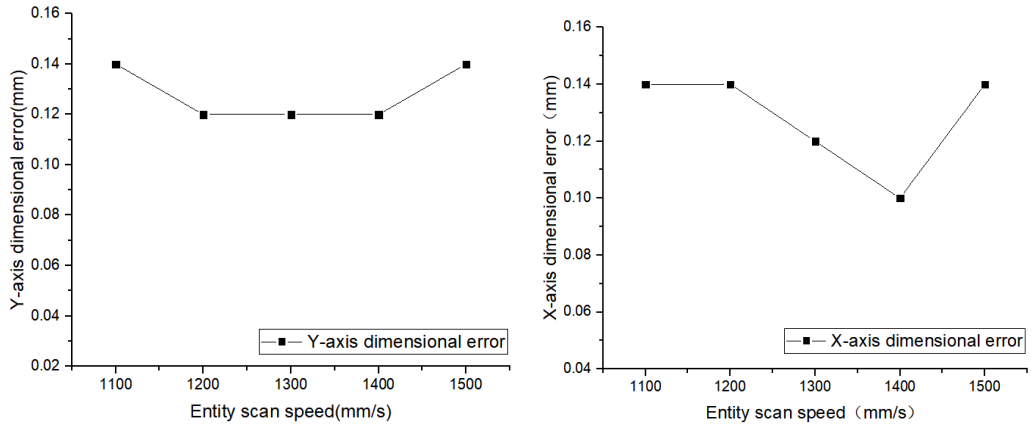

Fig. 3.14. Influence of solid scanning speed on X/Y axis dimensional error.

Fig. 3.14 shows the effect of solid scanning speed on the mean dimensional error in the X and Y directions of SLM molded parts. As can be seen from the figure, the size in both the X and Y directions shows a trend of slowly decreasing and then rapidly increasing with the increase of scanning speed. The difference between the maximum dimensional error and the mean minimum dimensional error in the X direction is 0.02 mm, and the difference between the maximum dimensional error and the mean minimum dimensional error in the Y direction is 0.04 mm.

When the scanning speed is too low, the laser beam scanning time is extended, the laser energy is larger and the time acting on the metal powder is longer, which can make the metal powder fully melt, but will produce different temperature gradients in the molten pool, so that the metal molten liquid spreads to the forming specimen around, the melting width and penetration depth are also larger, and there will be a large number of semi-melted and unmelted powder particles adhering to the forming surface and around the forming surface, so that the dimensional error becomes larger. When the scanning speed is too high, the laser beam acts on the surface of the metal powder for a short time, so that the metal powder melts quickly before heat exchange occurs, and then begins the scanning and forming of the next

layer, the melting width at this time is small, so the forming size error is small, and the dimensional accuracy is high. Overall, the scanning speed is 1500 mm/s, and the dimensional error of AlSi10Mg aluminum alloy SLM formed parts in the X and Y directions is smaller, with values of 0.12 mm and 0.10 mm, respectively, which has the highest dimensional accuracy.

3.3.3 Influence of scan distance on X/Y axis dimensional accuracy

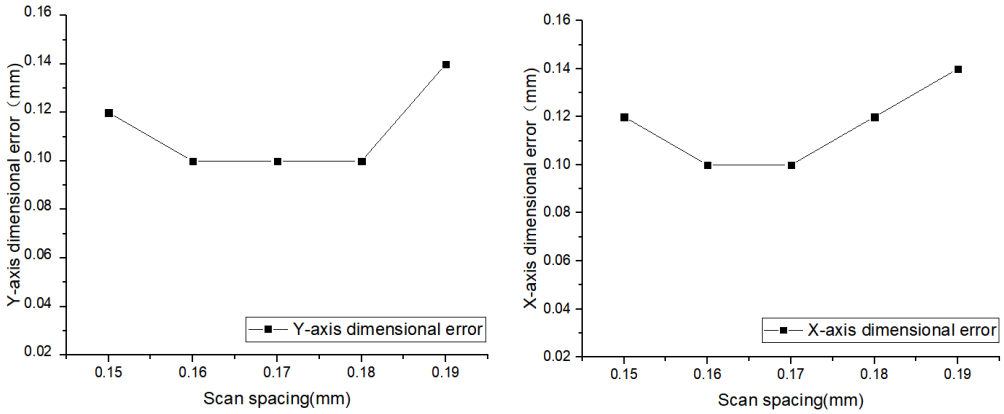

Fig. 3.15. Influence of scan spacing on X/Y axis dimensional error.

Fig. 3.15 shows the effect of the scan spacing on the average dimensional error in the X and Y directions of the SLM molded part. It can be seen from the figure that the dimensional error in the X direction and the dimensional error in the Y direction show a trend of first decreasing and then slowly increasing with the increase of the scanning spacing. The difference between the maximum dimensional error and the mean minimum dimensional error in the X direction is 0.04mm, and the difference between the maximum dimensional error and the mean minimum dimensional error in the Y direction is 0.04 mm.

When the scanning distance is too small, the lap rate will be relatively large, that is to say, there are more overlapping parts between the two adjacent melt channels, this part of the powder can be melted twice, although more metal powder can be fully melted, but the melting width and penetration depth during forming will increase to varying degrees, which

can make part of the semi-molten powder adhere to it, resulting in a larger dimensional error. When the scanning distance is too large, the lap rate between the two melt channels will be relatively small, the overlapping part will be less, the input energy is more evenly distributed, and will not cause a large amount of energy accumulation, although the powder melting amount is relatively small, but the melt channel width is small, basically there will be no metal powder adhering to the melted layer, thereby reducing the dimensional error and improving the dimensional accuracy. Overall, when the scanning spacing is 0.16 mm and 0.17 mm, the dimensional error of $AlSi_{10}Mg$ aluminum alloy SLM molded parts in the X and Y directions is smaller, with values of 0.10 mm and 0.10 mm, respectively, which has the highest dimensional accuracy.

3.4 Influence of process parameters on surface roughness of SLM forming $AlSi_{10}Mg/TiB_2$ alloy

The side surface quality of SLM forming parts occupies an important position in the surface quality of the whole part, especially for parts containing internal runners or spatial special-shaped surfaces, the quality of the side surface directly determines whether the formed parts are qualified, so it is necessary to study. This chapter examines the effects of contour process parameters such as profile laser power, profile scanning speed and scan spacing on the surface quality of specimens in SLM forming.

3.4.1 Effect of profile laser power on side surface roughness

Fig. 3.16 shows the effect of laser power on the mean Ra value of $AlSi_{10}Mg$ aluminum alloy SLM molded parts. It can be seen from the figure that with the increase of laser power, the surface roughness of $AlSi_{10}Mg$ aluminum alloy SLM molded parts first decreases and then gradually increases, the laser power is 350 W, and the minimum value of Ra is 5 μm.

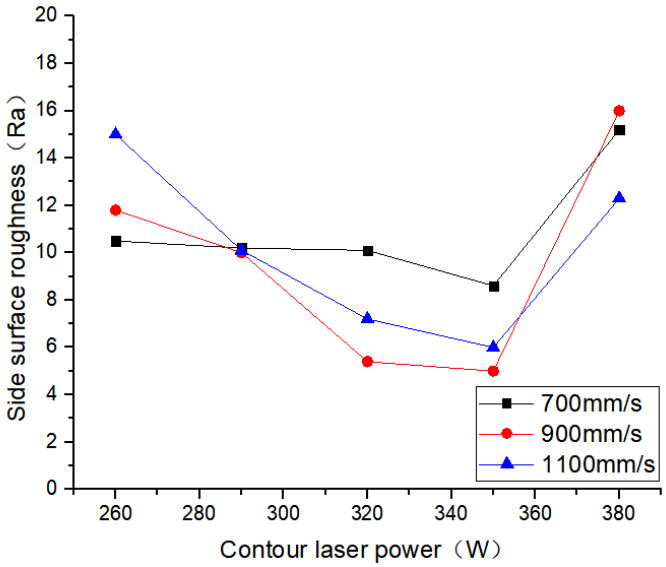

Fig. 3.16. Effect of profile laser power on side surface roughness.

3.4.2 Effect of contour scanning speed on side surface roughness

Fig. 3.17 shows the effect of scanning speed on the mean surface roughness Ra of SLM molded parts. It can be seen from the figure that with the increase of scanning speed, the smaller the surface roughness Ra of $AlSi_{10}Mg$ aluminum alloy SLM molded parts, the minimum surface roughness Ra is 6μm when the scanning speed is 900 mm/s, but after the scanning speed exceeds 900 mm/s, the roughness also increases with the increase of scanning speed.

When the scanning speed is small, the powder absorbs more energy per unit time, and it is easy to form too high energy, resulting in spheroidization and splashing of the powder, thereby affecting the surface roughness of the formed parts. With the increase of scanning speed, the energy absorbed by the powder per unit time decreases, the spheroidization and splashing of the powder decrease, and the surface roughness begins to decrease. When the scanning speed is 1000mm/s, the surface morphology of the formed part can be seen that due to the high scanning speed, low energy, small melt channel, it is difficult to observe the continuous and flat melting channel, and there is more powder adhered to the surface, which affects the surface quality. When the scanning speed is 1100 mm/s, it can be seen that

obvious unmelted powder and semi-melted powder can be observed on the surface, as well as a large number of raised balls, which will affect the surface quality of the molded part.

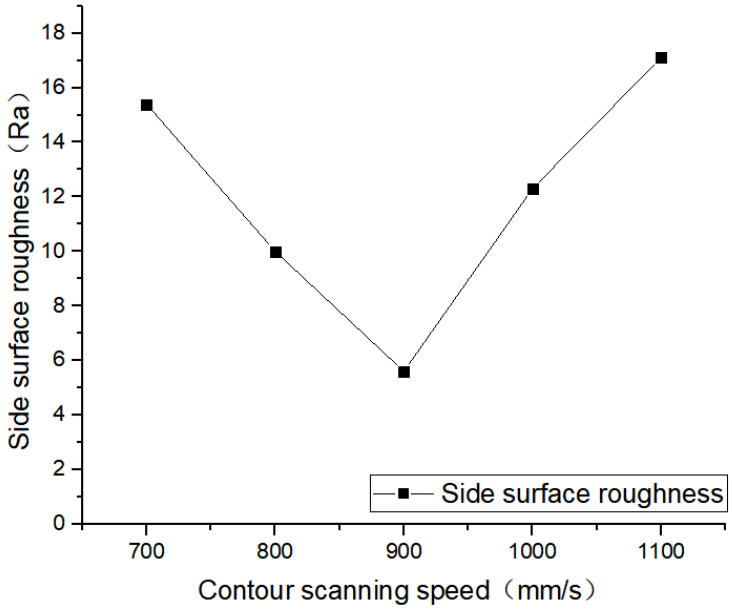

Fig. 3.17. Effect of contour scanning speed on lateral surface roughness.

3.4.3 Influence of scan spacing on side surface roughness

Fig. 3.18 shows the effect of the scan spacing on the mean surface roughness Ra of SLM molded parts. As can be seen from the figure, the surface roughness Ra does not change much with the increase of the scan spacing, and when the scan spacing is 0.17 mm, the minimum Ra is 5 μm.

Since the main factors affecting SLM forming are laser power and profile scanning speed, after determining the best laser power of 230W and the best contour scanning speed of 900mm/s, the influence of the scanning distance on the surface quality of the molded part is not very obvious, and the difference between the maximum Ra value and the smallest Ra value is less than 1 μm, which can basically ignore the influence of the scanning spacing.

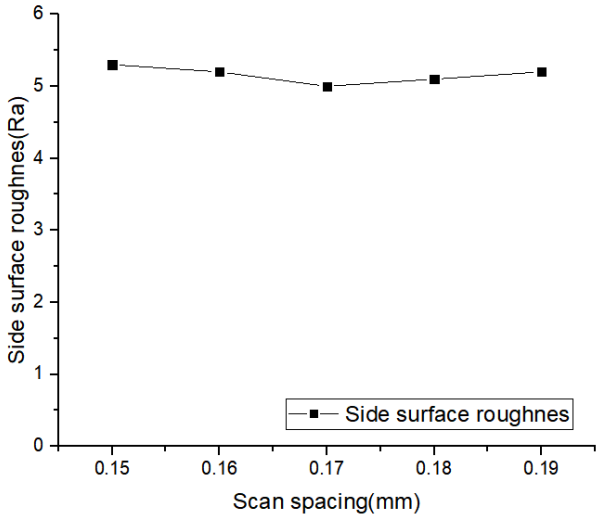

Fig. 3.18. Effect of contour scanning speed on lateral surface roughness.

Since the main factors affecting SLM forming are laser power and profile scanning speed, after determining the best laser power of 230 W and the best contour scanning speed of 900 mm/s, the influence of the scanning distance on the surface quality of the molded part is not very obvious, and the difference between the maximum Ra value and the smallest Ra value is less than 1 μm, which can basically ignore the influence of the scanning spacing.

3.4.4 Summary of this chapter

(1) The form of the powder will seriously affect the dimensional accuracy and surface roughness of SLM forming, for the powder used more than 30 times, the powder particle size is significantly increased, the powder accumulation characteristics deteriorate, the powder morphology has impurity particles, the oxygen content is high, and it is not easy to continue to use the printing directly.

(2) The orthogonal test analyzes the effects of scanning spacing, laser power and scanning speed on SLM forming dimensional accuracy and surface roughness, and obtains the following influencing factors: laser power> solid scanning speed> contour scanning speed> scanning spacing, and the optimal parameter combination is 0.17 mm, laser power

230 W, solid scanning speed 1500 mm/s, contour scanning speed is 900 mm/s, and scanning rotation angle is 67°.

3.5. Study of part structure on SLM forming dimensional accuracy and surface roughness

The previous chapter examined the dimensional accuracy of SLM molded square geometry (small squares), but printed parts are often assembled from multiple parts, and the structure of the parts is often composed of typical geometric features, such as round holes, square holes, cylinders, sharp corners, spherical shapes, curved surfaces, etc. Therefore, it is not enough to study the dimensional accuracy of SLM forming square geometry, this section makes a preliminary discussion on the molding ability and dimensional accuracy of other typical geometric features of SLM molding, which provides a theoretical basis for the three-dimensional structure design and process optimization of the assembly mechanism. The processing parameters used in this section of the experiment are shown in the table:

Table 3.3

The processing parameters

Laser power	Entity scan speed	Contour scan speed	Scan spacing	Scan rotation angle
230 W	1500 mm/s	900 mm/s	0.17	67°

3.5.1 Sharp corners

Sharp corner parts with angles of 15°, 30°, 45°, 60°, and 75° are formed horizontally and vertically. As shown in fig. 3.19, it is a schematic diagram and renderings of forming different angles. The surface roughness and dimensional accuracy of the specimen are measured separately.

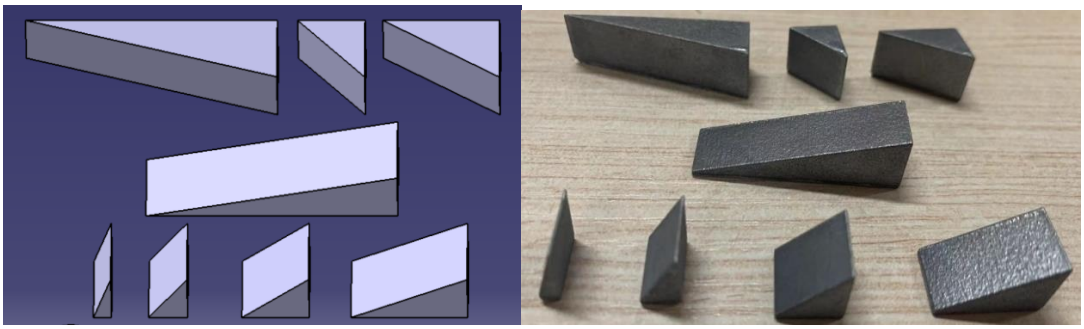

Fig. 3.19. Schematic diagram and effect diagram of forming triangular blocks with different angles.

When applying selective laser melting molding technology to mold parts, the parts to be formed are first designed in 3D drawing software, and then the part model is divided into sliced layers of a certain thickness, and then these slice layers are gradually stacked to obtain the formed part body. When the part to be formed is placed obliquely, the surface of the part becomes a step-shaped contour envelope instead of a continuous surface.

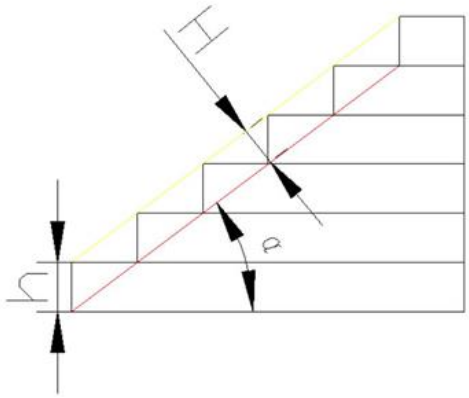

Fig. 3.20. Theoretical outline and actual contour.

As shown in fig. 3.21, the surface roughness of the vertically placed specimen first increases and then decreases, and when the angle exceeds 30°, the value of the surface roughness gradually decreases as the angle increases. However, the surface roughness is greater than that of flat forming, which is due to the stepwise effect of the part.

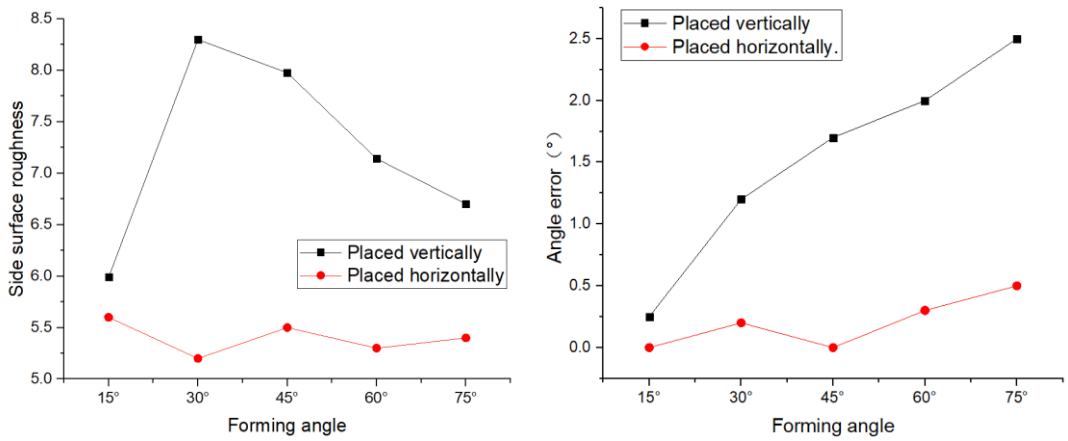

Fig. 3.21 Effect of placement on sample surface roughness and forming angle.

The angular error of the vertically placed formed part increases with the increase of the forming angle, and the angular error reaches 2.5° at 75°. This is also because of the step effect of the part, the molded part will be affected by the step effect when placed obliquely, the theoretical contour diagram is shown in fig. 4.2, where the oblique yellow line is the design profile, and the actual contour after molding is a jagged dark solid line part. If the forming thickness is h and the forming angle is α, the dimensional error caused by the step effect is: $H = h\cos\alpha$.

Through the above analysis, it can be seen that the dimensional error caused by the step effect is mainly related to the molding thickness and tilt angle, with the increase of the inclination angle and the decrease of the molding thickness, the smaller the dimensional error caused, theoretically when the forming angle is 90°, the structure with gap is placed vertically, at this time the step effect will disappear, but this will greatly consume printing time, affect processing efficiency, and even lead to molding failure.

3.5.2 Ring

Ring parts with wall thickness of 2mm and inner diameters of 2, 3, 4, 5, 6, 7 and 8 mm are formed horizontally and vertically. As shown in 3.21.

Fig. 3.22. Schematic diagram and renderings of forming rings of different radius.

As shown by fig. 3.22, the placement method has little effect on the error of the circularity of forming different rings, and the vertical placement is a little larger than the horizontal placement, but not more than 0.05°. However, the surface roughness of vertical placement will be smaller than that placed horizontally, the surface roughness Ra when placed vertically is about 5.5 μm variation, but the roughness when placed horizontally can reach Ra of 7.3 μm, but as the inner diameter of the ring increases, the surface roughness will also decrease, because when the size is larger, there can be better forming space, the molten pool can be better formed, the powder can be better heat transfer, the surface quality of the formed is better, and the surface roughness is reduced.

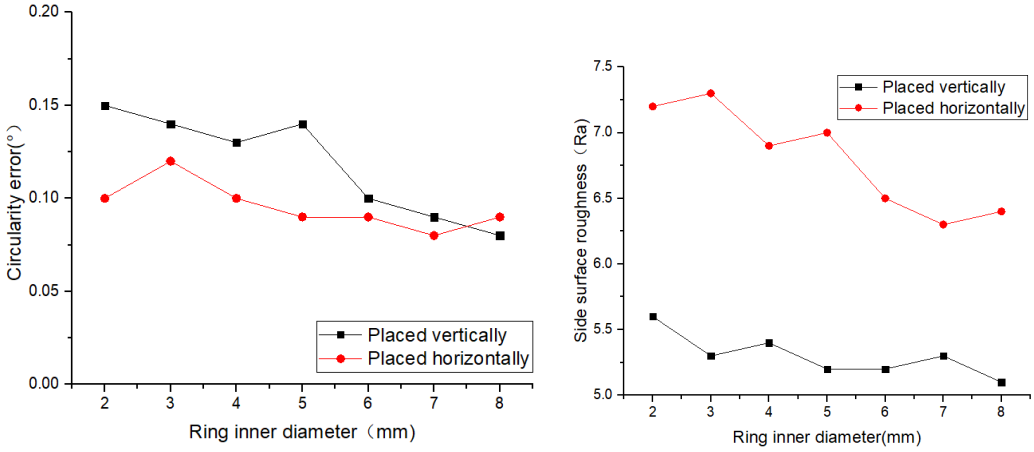

Fig. 3.23. Effect of placement on the surface roughness and forming angle of the ring.

For SLM forming, the size of the designed ring should not be too small when printing vertically, and for smaller rings, you can consider printing horizontally, which can better ensure the forming quality and roundness.

3.5.3 Summary of this chapter

(1) For parts with inclined surfaces, when placed vertically, the forming angle has a greater influence on the dimensional accuracy and surface roughness of SLM forming, and when the forming angle is about 30°, the surface roughness is up to 8.2 μm, but with the increase of this angle, the surface roughness also decreases, and the angle error becomes larger. Compared with vertical placement, the surface roughness is significantly reduced, and the forming angle error value is small and does not change much.

(2) For torus parts, the surface roughness when printing vertically is obviously better than horizontal placement, so when printing parts, for structures with more rings, horizontal placement printing is preferred.

PART 4. LABOR PROTECTION

Metal additive technology is an advanced manufacturing technology, the use of raw materials for metal powder, in the process of the experiment, will cause powder flying, easy to cause experimental fire, explosion and personnel inhalation safety hazards. In order to prevent the oxidation of the powder, the printing environment needs to be carried out under the protection of inert gas, this experiment adopts argon protection, argon storage method is in a closed cylinder, the use of operation is easy to cause the collapse of the cylinder, causing casualties, the placement of the cylinder needs to be under protective measures, in addition, when the printing room is filled with argon, minimize the release of argon into the laboratory, and the experiment needs to maintain a ventilated environment. The power supply used by the printing equipment is a high-voltage power supply, and during the experiment, pay attention to electrical safety [26].

During the experiment, masks must be worn when sifting powder and loading the powder into the equipment, this heavy metal can be inhaled into the body and cause serious damage to the human body. When inhaling dust, healthy people have a defensive function, and more than 90% of the inhaled dust can be excreted from the body, such as nasal hair and the inner wall of the respiratory tract can block and stick to the inhaled dust, so that it is discharged with nasal discharge and sputum[26,27]. If there is no dust prevention measures during the production process, long-term inhalation of dust in large quantities can irritate the mucous membrane of the upper respiratory tract, resulting in rhinitis, pharyngitis, laryngitis and bronchitis. Some people inhale grain dust to cause bronchial asthma.

4.1 Harmful and dangerous work factors

4.1.1 Risk one: Fire

The key to preventing a fire is to remember the three elements that start a fire (the "fire triangle"): fuel (metal powder or soot), ignition source (laser or spark), and oxygen. Although these metal printing devices are designed for laser and metal powder contact to

occur in an inert gas environment, it can be said to operate in a safe manner. However, as an operator, when handling dust or soot, you should avoid any ignition source environment. This is because two of the three elements have been met: fuel (powder or soot) and oxygen (in an open environment). Care needs to be taken to eliminate basic risks (including possible ignition risks such as smoking), and the main risk is electrostatic discharge (ESD), so some necessary protective equipment including anti-static wristbands is an effective way to avoid accidents.

Knowing the life cycle of powders can also help prevent the risk of accidents, which are transported to the processing site in canister packaging and finally collected as recycled powder (most powder) or as scrap recycled. It may seem quite complicated, but what must be understood and followed is the whole environment in which the powder exists: the powder trapped by the product, the powder to be recycled, the soot and powder trapped in the filter, and the accumulated powder accumulated by wiping and cleaning on gloves[27]. In addition, powder can accumulate on the internal hoses and shafts, and all deposited powder needs to be disposed of regularly.

Some basic safety measures should not be ignored, always wear gloves, goggles and protective clothing (lab coat) when using the machine. Even the simplest tasks like using a keyboard and mouse require attention to safety.

(a)Personal protective equipment (PPE)

PPE is a means of self-defense, in the event of a fire, can effectively protect life, according to different budgets, can be configured with different levels of protective equipment:

- Protective clothing: if using active metal, you can use a lab coat, covering the arm, protective gloves, antistatic belt;

- Standard PPE: respirator, nitrile gloves, mask, antistatic strap;

- Extended PPE: Standard PPE PLUS, Fireproof Grade Set, Fireproof Gloves;

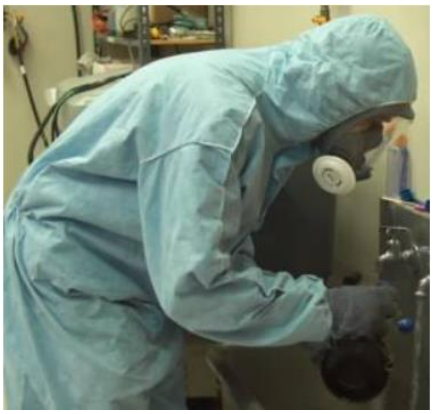

Fig. 4.1. Laboratory safety protective clothing.

(b) Extinguishing fires

There are several ways to extinguish fires, but it is clear that water and carbon dioxide are unsafe options for metal fires. To extinguish a fire, a metal fire needs to be a Class D fire extinguisher, which is a fire extinguisher rated for metal fires [28]. It is important to note that water can be dangerous for metal fires and require a professional fire brigade to make the best decision.

Fig. 4.2. Laboratory metal fire extinguishers.

(c) Powder storage

Fig. 4.3. Flammable fire cabinets.

When not used, the powder is stored in unopened jars, and when the jars are opened, it is better to store the opened jars in a flammable cabinet, which is not necessary for non-reactive alloys, but is necessary for reactive metal alloys.

4.1.2 Risk two: powder inhalation and exposure

The main way to reduce the risk of powder inhalation is the use of respirators [28]. These methods come in many forms, but for this process, the two most recommended are respirators with built-in masks, more preferably PAPR respirators, which provide positive pressure air, and respirator filters above N95 are recommended, but N100 is the most ideal choice.

When operating the machine, it is necessary to take care to always wear gloves and avoid contact with powder. This is also useful for minimizing the risk of carrying dust outside the metal 3D printer area:

Before you start working, you need to pay attention to your watch, watch jewelry and mobile phone.

After completing the work, you need to remove the protective jacket and then gently wipe your hands and elbows before handling any other items.

Consideration needs to be given to installing a layer of adhesive floor mat so that the operator can step on it when walking out of the room. Metal powder safety data

Fig. 4.4. Safety Data Sheets.

It is necessary to ensure that the powder supplier provides SDS (Safety Data Sheets) for all powders ordered and stores these forms in an easily found place for easy retrieval.

4.1.3 Risk three: inert gas asphyxiation

Inert gases (nitrogen or argon) are used to provide an environment against oxidation during powder processing, which are stored in gas cylinders (argon) or transported from generators (nitrogen). Leak-free facilities and stable equipment performance are critical, and when it is found that the required oxygen PPM level cannot be reduced in the construction room, or the gas composition fluctuates significantly, these may be related to the leakage of the inert gas. The user of the equipment must know the position of the gas valve and close it if necessary [26].

In order to prevent inert gas asphyxiation, an effective device is an oxygen sensor. This is an important sensor, especially in spaces where any devices that rely on inert gases, including 3D printers and furnaces, are installed. If the oxygen level falls below a safe value, an alarm is triggered to alert on-site personnel to evacuate immediately.

Fig. 4.5. Oxygen sensor.

4.2 Analysis of working conditions and formulation of protective measures

4.2.1 Fire prevention

1. It is strictly forbidden to use open flames in the laboratory, and smoking is not allowed in the laboratory.

2. When starting or shutting down electrical equipment, the switch must be tightly buckled or pulled properly to prevent the situation of unconnected. When using electronic instruments and equipment, you should first understand its performance, operate according to the operating procedures, and cut off the power immediately if the electrical equipment overheats or smells of paste.

3. When personnel leave the room for a long time or the power supply is interrupted, the power switch should be cut off, especially the power switch of the heating electrical equipment.

4. There should be no exposed wire heads in the laboratory; In the power switch box, it is not allowed to stack items to avoid electric shock or burning.

5. Pay attention to keep the wires and electrical equipment dry to prevent moisture and leakage of lines and equipment.

6. The laboratory is prohibited from using high-power electrical appliances except for experimental equipment, and the use of electric kettles is prohibited.

4.2.2 Safety of harmful substances and gases

1. All toxic substances and chemical agents shall be stored, distributed, and used in strict accordance with the category, and the remaining articles and residual substances shall be properly disposed of.

2. Practice personal hygiene and follow personal protective protocols, and do not eat or drink, smoke, or store food in containers that may be contaminated with poisons or in laboratories that may be contaminated with poisons. Wear protective clothing when working in a non-toxic environment that cannot be guaranteed; Wash your hands promptly after the experiment; Living clothes and work clothes should not be stored together.

3. When using laboratory equipment, open windows to maintain ventilation.

4. When it is found that there is an inert gas leakage in the laboratory, it should be stopped immediately, evacuate the personnel and quickly open the doors and windows or the extraction fan to eliminate it, check the leakage and repair it in time. All equipment is prohibited until completely excluded.

5. Before leaving work or leaving the laboratory, pay attention to check whether the used instruments are completely closed, and if it needs to be continuously opened, a special person needs to work overtime to take care of it.

6. It is strictly forbidden to place flammable and explosive materials in the metal powder storage point.

4.2.3 Gas cylinder safety

1. If the cylinder body is defective, the safety accessories are incomplete or damaged, and the safe use cannot be guaranteed, it must not be sent to the filling gas again, and it should be sent to the relevant unit for inspection before it can be used.

2. Gas cylinders must be classified and stored separately, and fixed and stable when placed upright; The cylinder should be kept away from heat sources to avoid exposure to sunlight and strong vibration.

3. When using gas cylinders, the operator should stand in a position perpendicular to the gas cylinder interface. It is strictly forbidden to knock and impact during operation, and often check whether there is air leakage, and pay attention to the pressure gauge reading.

4. Gas cylinders should be sent for inspection regularly to ensure the quality of gas cylinders. The inert gas cylinder storage point should have good ventilation conditions.

4.3 Fire Safety Rules for Workplaces

In order to ensure the safety of the experimenter, the experimental operator must master the correct operation of the experiment, and the experiment must ensure that two people are present at the same time, and the experiment needs to be guarded. Laboratory safety facilities must meet national laboratory safety specifications, and experiments are prohibited in places where safety facilities are not perfect.

PART 5. ENVIRONMENTAL PROTECTION

5.1 Environmental protection applications of metal additive manufacturing in various fields

Metal additive manufacturing technology (also known as "3D printing") has been hailed as one of the disruptive technologies leading to industry change. Different from the traditional subtractive process of cutting and assembling raw materials, additive manufacturing technology uses digital model files to melt, extrude, sinter, light solidify and other combinable materials such as metal powder and plastic to accumulate point by point, line by line and surface by surface. make actual objects [30]. Additive manufacturing creates complex structures from digital models, saving material, allowing for flexible design and personalization. With the continuous application of new materials and the development of additive manufacturing technology, additive manufacturing technology is widely used in aerospace, biomedical, transportation, smart wear and other fields [32].

Most traditional manufacturing techniques are subtractive, which means cutting into a piece of material or producing and filling an injection mold. This creates waste, some of which can be reused, but some that cannot. In any case, even if the material is recycled, it must be reprocessed. Additive processes, on the other hand, involve no molds and no engraving waste. Much progress has also been made in the ability to reuse leftover materials. For example, one of HP's equipment can recycle up to 80 percent of excess powder. As an industry, we have high expectations for sustainable innovation in materials.

5.1.1 Application of Metal Additive Manufacturing Technology in Aerospace Field

Aerospace is an early field of metal additive manufacturing, and it was early applied to titanium alloy brackets. The aluminum alloy powder laser additive manufacturing technology is used to make the aircraft central flange member, which can improve the

metallurgical quality of the material, and has been practically applied in domestic aircraft [33].

The cost of aluminum alloy materials is high. For the production of small batches of trial parts, in the traditional manufacturing process, it is necessary to consume a whole piece of aluminum alloy raw materials, resulting in a large amount of waste. Using additive manufacturing technology, aluminum alloy powder can be recycled, theoretically resulting in zero waste. And can complete the manufacturing process of the product in a short time.

Fig. 5.1. Metal additive manufacturing aircraft engine.

5.1.2 Application of metal additive manufacturing technology in the field of biomedicine

Due to the complex structure of biomaterials, the varying needs of patients, and the need for mass production, additive manufacturing technology is very suitable for manufacturing biomaterials.

The application of metal additive manufacturing technology in the manufacture of dental prostheses mainly focuses on metal base crowns, metal stents and implants for removable partial dentures. The metal-ceramic bonding force of the cobalt-chromium alloy bottom crown made by metal additive manufacturing is close to or even higher than that of traditional production; due to the fast cooling rate, compact structure and defect-free metal

additive manufacturing, the strength of the cobalt-chromium alloy produced by metal additive manufacturing is higher than that of traditional casting; With proper computer-aided design and parameter setting, cobalt-chromium alloys manufactured by metal additive manufacturing can achieve good abutment adhesion[34].

Metal additively manufactured cobalt-chromium alloy removable partial denture metal stents are close to traditional stents in fit and function, but have better microstructure. Due to factors such as rapid cooling and crystal phase composition, titanium alloy implant stents made by metal additive manufacturing technology have higher density and hardness, light structure and good biocompatibility.

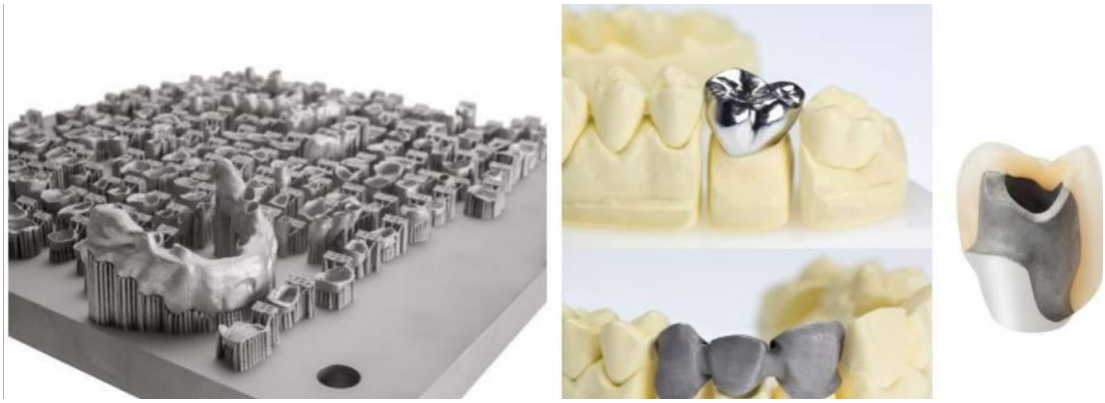

Fig. 5.2. Application of metal additive manufacturing technology in the medical field.

5.1.3 Application of metal additive manufacturing technology in the field of transportation

The application of metal additive manufacturing in the field of rail transit is mainly in the production of parts and the additive repair of damaged parts. Metal additive manufacturing rapidly melts and solidifies under a high-density heat source, and the microscopic grains of the manufactured parts are fine and uniform, and the solute segregation is small. Foreign locomotive companies have used metal additive manufacturing to form train bearings with complex structures in the follow-up maintenance

of trains to improve the bearing's anti-vibration performance and wear resistance, and use stainless steel additive to manufacture rail train bogie anti-roll torsion bar mounts. Based on the optimized design, a mounting seat with a bionic structure is printed, which reduces the weight by 70% and reduces the energy consumption of the car while ensuring the original performance.

Using metal additive manufacturing technology to manufacture engine cylinder heads, the products formed have high density, no cracks and shrinkage holes that may occur during casting, and the performance is close to forgings, but the series of processes such as mold opening and pouring in traditional manufacturing are omitted. It solves the problem of time-consuming production of cylinder heads in small batches. The engine block and gearbox housing are traditionally produced by casting. Combining metal additive manufacturing technology and casting can reduce costs and shorten construction periods while ensuring product quality.

Fig. 5.3. Application of metal additive manufacturing technology in the automotive field.

5.2 Recycling and Utilization of Metal Additive Manufacturing Materials

The cost of additive manufacturing of high-end materials has continued to increase in recent years as equipment manufacturers push traditional metal powder producers to offer

specialty powders designed for aerospace, biomedical and transportation applications. Based on this, the recyclability and recycling of powders becomes even more important. The 3D Printing Technical Reference will specifically address some of the challenges of powder recovery and recycling in metal additive manufacturing, especially ways to improve powder reusability [35].

5.2.1 Differences in powder degradation behavior

Different types of powders exhibit different performance changes after one or more printing cycles. Inconel 718 has good chemical stability during recycling, but is limited by the physical properties of morphology and flow when evaluating reusability. When these materials melt at higher temperatures, the material around the melt deforms and sinters together, which makes the powder particles larger and unusable. The titanium alloy powder is more likely to absorb oxygen, and the high oxygen content of the powder will lead to printing failure. Therefore, the oxidation of the powder must be always paid attention to, and the number of times of its use will be greatly limited.

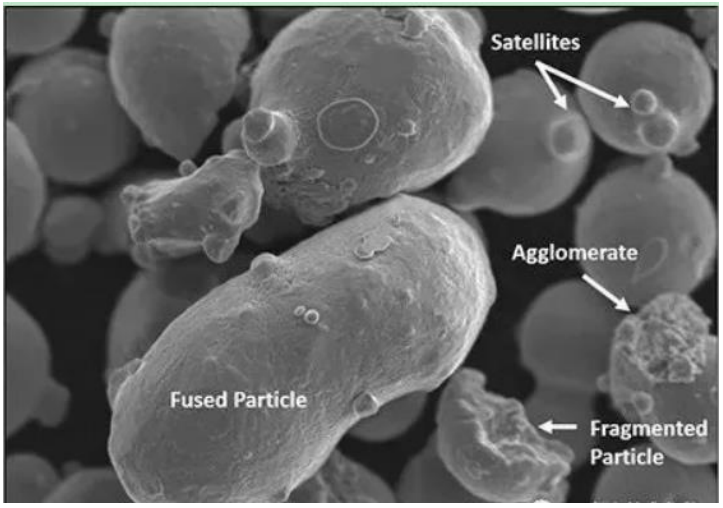

Fig. 5.4. Degradation of metal powder after repeated use.

In a high-temperature material recyclability study, researchers analyzed powders from multiple SLM printing cycles to understand the effect on powder and part performance. During multiple prints, the satellite powder attached to the larger powder particles begins to separate into smaller individual particles. At the same time, the powder particles begin to fuse together to form agglomerates, in which the particles break down into incomplete fine particles. All of these affect the flowability and bulk density of the powder, broaden the particle size distribution of the powder and increase the oxygen content of the powder. However, after 13 consecutive cycles using the same batch of powder, the powder still met the ingredient specification for reusability [32].

5.2.2 Improve the reusability of powders

Improving the reusability of metal powders requires the identification of qualified technologies to repair off-spec powders and make them reusable. A popular method right now is to mix the new powder with the old powder before each build. It can reduce the oxygen content in the powder, and can also control the physical properties such as particle size distribution and bulk density of the powder. However, there is currently no established mixing standard, and users rely on experience to determine the optimal ratio, and these attempts often vary depending on the material used and the type of part manufactured.

Another reasonable repair technique is to use an induction plasma process, which can send irregularly shaped and less fluid powders through a powder feeder into an induction plasma, where it is rapidly heated and melted by high temperature to form droplets, agglomerated into a spherical shape under the action of surface tension, and re-solidified during the falling process, thereby obtaining spherical powder particles. This method can improve properties such as powder flow and bulk density [34].

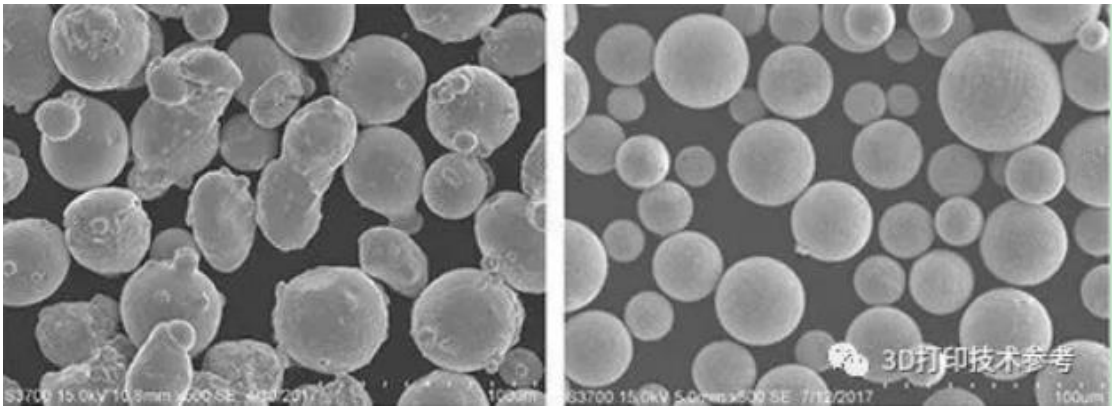

Fig. 5.5. Comparison before and after induction plasma treatment.

By remelting and solidifying powder particles to reduce porosity, increase powder density, and selectively remove impurities to improve powder purity by increasing plasma melting temperature and modifying shielding gas. Research organization EWI has conducted some early studies using this method, but further testing will have to be carried out to assess the feasibility of powder repair.

REFERENCES

[1] Xie Jianxin. High-performance aluminum alloy materials for aerospace and modern transportation[C]. 2019 China Aluminum Processing Industry Annual Conference and China (Zouping) Aluminum Processing Industry Development Summit Forum Proceedings. China Nonferrous Metals Processing Industry Association, Zouping Municipal People's Government: China Nonferrous Metals Processing Industry Association, 2019: 34-57.

[2] ZHAO Zhiguo, Berlin, LI Li, et al. Development status and research progress of laser selective melting forming technology[J]. Aeronautical Manufacturing Technology, 2014, 463(19): 46-49

[3] HU Fenglan, YAO Junhong, QI Xindan. Interchangeability and technical measurement basis[M]. Higher Education Press, 2010.

[4] KRUTH, J. Selective laser melting of iron-based powder[J]. Journal of Materials Processing Technology, 2004, 149(1-3): 616-622.

[5] Over C , Meiners W , Wissenbach K , et al. Selective laser melting: a new approach for the direct manufacturing of metal parts and tools. 1st International Conference on Laser Assisted Net Shape Engineering, Germany: Frankfurt, 2001.

[6] YANG Yongqiang, WU Weihui, LAI Kexian, et al. Laser melting direct rapid prototyping process for metal parts selection and its latest progress[J]. Aeronautical Manufacturing Technology, 2006(02): 73-76+97.

[7] TANG Jiali, XU Zhangtao. Range analysis and ANOVA in orthogonal test[J]. Secondary School Mathematics, 2017(09): 31-34.

[8] Simchi A. Direct laser sintering of metal powders: Mechanism: kinetics and microstructural features[J]. Materials Science and Engineering, 2006(01): 48-158.

[9] Gu D, Hagedorn Y.C., Meiners W, et al. Densification behavior, microstructure evolution, and wear performance of selective laser melting processed commercially pure titanium[J]. Acta Materialia, 2012, 60(09): 3849-3860.

[10] Kruth J.-P., denbroucke B., erenbergh J.V., et al. Benchmarking of different SLS/SLM process as rapid manufacturing techniques[J]. Int.Conf.Polymers & Moulds Innovations(PMI), Gent, Belgium, 2005(04): 20-23.

[11] Vandenbroucke B , Kruth , Jean-Pierre. Selective laser melting of biocompatible metals for rapid manufacturing of medical parts[J]. Rapid Prototyping Journal, 2007, 13(04): 196-203.

[12] Yang Xiongwen. Research on dimensional accuracy of laser selective melting molded parts and its application in direct manufacturing of assembly-free mechanism[D]. Guangzhou:South China University of Technology, 2015.

[13] Bourell D , Spierings A B , Herres N , et al. Influence of the particle size distribution on surface quality and mechanical properties in AM steel parts[J]. Rapid Prototyping Journal, 2011, 17(03): 195-202.

[14] Qian Kun. Experimental study on dimensional accuracy and surface quality of selective laser melting molding structure with gap[D].Yanshan University,2021.DOI:10.27440/d.cnki.gysdu.2021.001930.

[15] Zhang Luo. Study on the dimensional accuracy of typical structure of Ti6Al4V by laser selective melting[D].Huazhong University of Science and Technology,2019.DOI:10.27157/d.cnki.ghzku.2019.004751.

CHEN Guangxia, WANG Zemin, GUAN Kai, et al. Effect of Process Parameters on Surface Roughness of SLM Laser Rapid Spring[J]. Manufacturing Technology and Machine Tools, 2009(12): 86-89.

[17] Wang Li. Study on properties of selective laser melting and forming metal parts[D]. Wuhan:Huazhong University of Science and Technology, 2012.

[18] Dadbakhsh S , Hao L , Jerrard P G E , et al. Experimental investigation on selective laser melting behaviour and processing windows of in situ reacted Al/Fe2O3 powder mixture[J]. Powder Technology, 2012, 231(07): 112-121.

[19] Amend P , Pscherer C , Rechtenwald T , et al. A fast and flexible method for manufacturing 3D molded interconnect devices by the use of a rapid prototyping technology[J]. Physics Procedia, 2010(05): 561-572.

Yuan Xuebing, Wei Qingsong, Wen Shifeng, et al. Study on selective laser melting of AlSi10Mg alloy powder[J]. Hot Working Technology, 2014(4): 91-94. [61] Ma Wei. Study on surface quality and density of GH4169 formed parts by selective laser melting[D]. Harbin: Harbin Institute of Technology, 2017

[21] Singh S , Sharma V S , Sachdeva A . Optimization and Analysis of Shrinkage in Selective Laser Sintered Polyamide Parts[J]. Materials and Manufacturing Processes, 2012, 27(6): 707-714.

[22] Kochan D , Kai C C , Zhaohui D . Rapid prototyping issues in the 21st century[J]. Computers in Industry, 1999, 39(1): 3-10.

[23] Wiedemann B , Jantzen H A . Strategies and applications for rapid product and process development in Daimler-Benz AG[J]. Computers in Industry, 1999, 39(1): 11-25.

[24]DONG Peng, LI Zhonghua, YAN Zhenyu, et al. Research status of aluminum alloy laser selective melting and forming technology[J]. Applied Lasers, 2015, 35(05): 91-95.

[25] DENG Qilin, LI Yanming, FENG Liping, et al. Laser near-shape manufacturing technology[J]. Electroprocessing, 1999(06): 39-42.

[26] KRUTH, J. Selective laser melting of iron-based powder[J]. Journal of Materials Processing Technology, 2004, 149(1-3): 616-622.

[27] Ge Hongyan. Effect of melting and heat treatment process on the performance of ZL114A alloy casing[D]. Harbin:Harbin University of Science and Technology, 2006.

[28] Wang Xiaojun. Study on selective laser melting process parameters and properties of Al-Si alloy[D]. Beijing:China University of Geosciences, 2014.

[29] Kobayashi T . Strength and Fracture of Aluminium Alloys[J]. Materials Science Forum, 2003, 426-432: 67-74.

[30] Sercombe, T B . Rapid Manufacturing of Aluminum Components[J]. Science, 2003, 301(5637): 1225-1227.

[31] ZHAO Zhiguo, Berlin, LI Li, et al. Development status and research progress of laser selective melting and forming technology[J]. Aeronautical Manufacturing Technology, 2014, 463(19): 46-49.

[32] KRUTH J P . Part and Material Properties in Selective Laser Melting of Metals[C]. Proceedings of the 16th International Symposium on Electromachining. Non-traditional Machining Society of CMES: Chinese Society of Mechanical Engineering, 2010: 5-16

[33] XIANG Dan,BAI Yanhong,WANG Geng,GAO Peihong,ZHANG Zhicheng. Laboratory Science,2022,25(03):213-216.)

[34] Yang Minfang. Research on the construction of laboratory safety management standards[J].Popular Standardization,2022(02):37-39.)

[35] Chang Shenghua, Weng Xiuxiu, Hou Fujiang. Analysis and research on safety management in university laboratories[J].Experimental Technology and Management,2016,33(01):229-231.DOI:10.16791/j.cnki.sjg.2016.01.061.

[36] ZHANG Yubiao,WANG Huijun. Gansu Metallurgy,2020,42(04):127-129.DOI:10.16042/j.cnki.cn62-1053/tf.2020.04.038.

[37] TANG Jinjing,YAN Wei,LIAO Qi,YANG Xianyong,JIANG Shuyu. Experimental Technology and Management,2018,35(04):256-257+266.